Kan Wu

Developing Non-fouling Zwitterionic Coatings for Biomedical Application

Kan Wu

A dissertation

submitted in partial fulfillment of the

requirements for the degree of

Doctor of Philosophy

University of Washington
2020

Reading Committee:

Shaoyi Jiang, Chair

Buddy D. Ratner, Chair

Rene Overney

Program Authorized to Offer Degree:
Chemical Engineering

University of Washington

Abstract

Developing Non-fouling Zwitterionic Coatings for Biomedical Application

Kan Wu

Chair of the Supervisory Committee:

Professor Shaoyi Jiang

Porfessor Buddy D. Ratner

Chemical Engineering

During the past decades, the demand for biomaterials with good biocompatibility is increasing with the rapid development of advanced medical technologies, such as biosensors, implantable chips, hemodialysis and biopharmaceutical application. Currently, high biocompatibility can be achieved by hydrophilic polymers, such as poly(ethylene glycol) (PEG), polysaccharides, and zwitterionic polymers. These hydrophilic polymers can form a stable hydration layer through hydrogen bonding with water molecules in their aqueous environment and these hydration layers further prevent non-specific protein adsorption onto, and immune recognition of, the material surfaces. Among all hydrophilic materials, zwitterionic carboxybetaine (CB) distinguishes itself from the rest for its exceptional biocompatibility, superior hydration capability, low immunogenicity, and high stability as well as its potential for further functionalization. However, a reliable method to successfully introduce the biocompatible polymer onto the target surfaces still persists as a challenge. For example, “graft-from” methods, exemplified by surface-initiated atom

transfer radical polymerization (SI-ATRP) can provide a dense layer but the harsh polymerization conditions and high cost impeded its large scale industrialization. On the other hand, "graft-to" methods are economic and realistic but their performance is highly surface-dependent and needs challenging optimization. There is a realistic demand to develop facile yet effective coating techniques.

In this thesis, we aim to develop a universal coating technique that can have the advantages of "graft-to" and "graft-from" methods, is facile to use and generates a dense coating layer. This coating method can create an excellent biocompatible layer onto all surfaces thought a simple dip-coating process. To achieve this goal, we developed a series of (PCB)m-(DOPA)n (m=1,4 and n=1,2,4) conjugates with different combinations of polycarboxybetaine (PCB) and mussel-inspired binding groups (DOPA) groups to find out what is the optimal molecular structure for modifying surfaces. We found that the structure of the conjugates affects their coating performance: a star-shaped PCB chain structures combined with multiple DOPA groups can significantly increase the coating performance. In order to test the universal-protection ability of the molecules, we next applied this coating material on to respiratory devices to test the performance of a coating in an *in vivo* sheep and rabbit study. We demonstrated that through our universal coating technique, the PCB-DOPA coating can significantly improve the respiratory device lifespan from 4 hours to 35 hours and can reduce thrombosis in sheep studies.

Expanding upon the well-known non-fouling ability of PCB coatings, we developed a new conjugate that can covalently immobilize bovine serum albumin antibody (anti-BSA) and fibrinogen antibody (anti-Fg) onto the PCB polymers. This coating was then applied onto a paper-based sensor surface *via* a "graft-to" immersion process to render the surface with both nonfouling and protein functionalizable properties. The coated paper sensor showed accelerated diffusion of analytes and improved sensitivity of glucose detection, particularly in real-world complex media such as human blood serum. Lastly, we propose a new

method to detect the complement activation level in the blood exposed to biomaterials. This detection method can improve the current measuring techniques by achieving a more accurate measurement.

By tailoring and molecule structure and chemistry, we have explored the strategies to improve the performance of non-fouling coating molecules. This new zwitterionic coating is developed to address major challenges associated with blood compatibility. These new molecules can not only greatly improve the life span and performance of medical devices, but also reduce the unfavorable immune response compare to current so-called “bio-inert” materials.

Acknowledgements

For all the works presented here, the author would like to thank his advisors, Professor Shaoyi Jiang and Professor Buddy Ratner for support, inspiration and funding for all presented works. The author would like to thank all the members of Jiang research groups for their kind help and discussion. The author would also like to express his special appreciation to his family, Jianfeng and Juan for their unflagging support.

Table of Contents

List of Tables

List of Schemes

List of Figures

Chapter 1 Introduction

Biomaterials are commonly used in various types of implanted devices, such as hemodialysis, catheters, stents, and biosensors.[1] However, almost all biomaterials used in

blood-contacting medical devices activate the host–immune system to a certain degree. [2-3] The crosstalk between coagulation, fibrinolysis, and inflammation caused by the non-specific protein fouling on foreign material surfaces impedes the life span or performance of implanted devices. [3] One common solution is introducing a bio-inert coating onto the device surfaces to increase the biocompatibility of medical devices. However, a reliable method to successfully introduce such biocompatible polymer onto the target surfaces is still challenging. “Graft-from” methods usually can provide an effective and dense coating, but the reaction condition is harsh and usually needs to be oxygen-free.[4] On the other hand, “graft-to” methods, exemplified by randomly copolymerizing hydrophobic or photo-reactive groups are easy to perform and low cost, but their coating performance depends on the chemical nature of target surfaces and requires surface-specific optimizations.[4]

Success in introducing biocompatible coatings onto the target surfaces is not the end of the story. Poor choose of materials can bring new issues after solving the old one. For example, polyethylene glycol (PEG) is a water-soluble synthetic polymer consisted of ethylene glycol (-CH2-CH2-O-) repeating units and has been recognized as a classic “non-fouling” material that resists non-specific protein adsorption, and is used to coat various surfaces of biomedical devices. Even though PEG is widely considered as one of the most common polymer coating materials for biomedical applications, inappropriate usage of PEG can introduce undesired immunogenic problems. Complement reaction is a critical part of the human immune system, especially in the innate immune system. Inappropriate activation of complement reaction can cause severe reactions such as hypertension, arterial calcification, and cardiometabolic risk. The free hydroxyl groups on the PEG chain ends can form a covalent bond with nascent C3b and trigger unexpected complement reaction.[5] However, besides PEG, other hydrophilic materials also bear the same issue despite the lacking of systematic studies.

In this dissertation, we discuss how to achieve a non-fouling surface coating through a simple dip-coating method using a polymer conjugate comprising of DOPA molecules and PCB polymers. We then applied the conjugate molecules on to the respiratory devices for *in vivo* sheep and rabbit studies. In addition, we propose a new method to quantitatively measure the immunogenicity of current prevailing bio-compatible coating materials, which can provide a fair and direct comparison on their complement activation level. In Chapter 2, we study the effect of molecular structure on the coating performance, to achieve this goal, we prepared a series of zwitterionic PCB-DOPA conjugates of (PCB)m-(DOPA)n with the different number of PCB chains (m) and DOPA binding groups (n). A linear PCB polymer version (m=1) versus a branched polymer chain version (m=4) was synthesized and combined with different numbers of DOPA groups (n=1,2,4) **(Figure 2.1).** Conjugates with different molecular architectures (n=1,2,4 and m =1,4) were designed and synthesized using the concept of modular synthesis. The efficiencies of different molecules coated on commonly used biomaterial surfaces were quantitatively compared using an enzyme-linked immuno sorbent assay (ELISA) and a bacteria attachment test with Staphylococcus aureus. We found that the increase of DOPA binding groups can significantly increase the binding affinity of coating molecules and the star-shaped polymer structure can reduce the steric hindrance without compromising the PCB content, and thus can achieve the best surface coating performance. This resulting "Janus" form molecule (n=4, m=4) showed the lowest protein adsorption of 19.5 ng/cm2 against 100% human serum from measurements with a surface plasmon resonance (SPR) sensor, which is the lowest result ever achieved by any surface-independent "graft-to" zwitterionic coating, to the best of our knowledge.

In chapter 3, artificial lung prototype devices coated with e PCB-DOPA conjugates as well as their uncoated control devices were attached in parallel within a veno-venous sheep extracorporeal circuit with no continuous anticoagulation (N = 5 circuits). This part of work was done by collaboration with Dr. Rei Ukita and Dr. Keith Cook in the Carneige Melon

University. Our lab was focusing on the surface treatment of the artificial lungs' prototypes while Dr. Rei Ukita was in charge of the animal study part. The results indicated that the PCB-$(DOPA)_4$ approach showed the least increase in blood flow resistance and the lowest incidence of device failure over 36-hours. Another 4-hour rabbit study with a veno-venous micro-artificial lung circuit at a higher activated clotting time of 220–300 s (N = 5) proved that PCB-$(DOPA)_4$ reduced fibrin formation ($p = 0.06$) and gross thrombus formation by 59% ($p < 0.05$).

In Chapter 4, we prepared a version of PCB-$(DOPA)_4$, which has a reactive carboxylic group on each repeating unit of the PCB chain. We applied the coating onto a paper-based sensor surface *via* a simple "graft-to" immersion process to render the surface with both nonfouling and protein functionalizable properties. The coated paper sensor showed both increased analyte diffusion rate and improved sensitivity of glucose detection in human blood serum. The capability of PCB-$(DOPA)_4$ modified paper sensor for specific antigen-antibody detection was demonstrated via the covalent immobilization of bovine serum albumin antibody (anti-BSA) and fibrinogen antibody (anti-Fg) onto the PCB-coated surface *via* a simple 1-ethyl-3-(3-dimethylaminopropyl)-carbodiimide and N-hydroxysuccinimide (EDC/NHS) chemistry.

A successful biocompatible material should have not only good fouling-prevention ability, but also low immunogenicity. Complement reaction is a common immunogenic problem in the field of biomaterials. Though a lot of *in vitro* studies have been conducted to quantify complement activation on material surfaces, there are still two major problems among these studies. First, the testing methods used are still far from flawless as their results will be easily affected by environmental factors like liquid-air interface and other surfaces. Second, the methods used by different groups lack consistency so there is a lack of direct and standard comparison between commonly used biocompatible polymers which

is urgent for material scientists. In Chapter 5, we aim to solve both of these problems at a time. In this study, we tested 3 groups of commonly used biocompatible polymers with different functional groups, which are amino-based, zwitterionic-based, and hydroxyl-based polymers. All these materials were made into polymer hydrogels with 20 %wt solid content to make sure the all tested polymer samples have the same amount of functional groups. All the wells possess the same shape and same volume. During the incubation, all samples were sealed to eliminate the potential evaporation and air activation. Zwitterionic-based materials, including CB and N-oxide (TMAO) shows the lowest complement activation due to their excellent non-fouling ability. Hydroxyl-based polymers such as ethylene glycol methacrylate (EGMA), N-(2-Hydroxypropyl) methacrylamide (HPMA), and polyvinyl alcohol (PVA) exhibits varying complement activation degrees, even though they are considered as bio-inert materials.

Chapter 2 A multivalent Janus copolymer for universal anti-fouling coating

To understand the structure–property relationship in a simple dip coating method, we developed a group of $(PCB)_m$-$(DOPA)_n$ (m=1, 4 and n=1, 2, 4) conjugates based on the marriage of nonfouling polycarboxybetaine (PCB) and surface-adhesive mussel-inspired binding dihydroxyphenylalanine (DOPA) groups as a surface-independent non-fouling

coating material. The structural parameters (e.g., molecular weight and composition) of these $(PCB)_m$-$(DOPA)_n$ conjugates were precisely controlled using the concept of "modular synthesis". The conjugate with a multi-valent binding sites (n=4) to increase binding strength and a star-shaped polymer structure (m=4) to reduce steric hindrance was demonstrated to have the highest surface packing density and the best nonfouling performance. The protein adsorption of 19.5 ng/cm^2 against 100% human serum was measured with a surface plasmon resonance (SPR) sensor. To the best of our knowledge this is the lowest achieved by any "graft-to" coating. This study demonstrated that a clear separation between the bio-inert polymer block and the surface-binding block can reduce steric hindrance between conjugates and increase the effective exposure of binding groups. The molecular-level understanding of structural effects on coating performance from this library of conjugates will guide the design of effective "graft-to" coatings.

2.1 Introduction

Non-fouling or bio-inert surfaces are highly desirable for the development of medical devices, biosensors, implantable chips and even marine coatings.[1] Bio-inert polymers, such as poly(ethylene glycol) (PEG) and zwitterionic polymers, have been introduced onto surfaces either by "graft-to" or "graft-from" methods.[2] Due to the demanding polymerization conditions as well as the additional pre-coating processes necessary with a surface-specific initiator for all "graft-from" methods, "graft-to" methods presents to be more practical for large-scale applications.

For "graft-to" methods, the most popular choice is to prepare a polymer coating through randomly co-polymerizing binding monomers [e.g., butyl methacrylate (BMA), catechols or charges] with bio-inert monomers [e.g., ethylene glycol (EG), 2-hydroxyethyl

methacrylate (HEMA), and 2-methacryloyloxyethyl phosphorylcholine (MPC) monomers]. Although these copolymers can reduce nonspecific protein adsorption, it is hard to achieve very low fouling against undiluted human serum or plasma, possibly due to the exposure of hydrophobic binding groups across the bio-inert polymer layer as they are randomly polymerized together. Moreover, current "graft-to" methods are also limited to surface binding groups that are highly surface-dependent, such as thiol to gold, silanes to silica/glass, and phosphate to metal oxide.[1a] Waite and Israelachvili et al. discovered that catechol groups in mussel foot proteins are responsible for the adhesion of mussels onto distinctive surfaces using a variety of mechanisms including H-bonding, coordinate bond, π-π stacking and van der Waals' force induced hydrophobic interaction.[3] This finding made it possible to develop a mussel-inspired universal coating material based on catechol groups, such as dihydroxyphenylalanine (DOPA), norepinephrine, DOPAmine, and tannic acid.[4] Lee et al. developed a universal coating method involving a poly-DOPAmine layer as the anchoring layer.[5] This pre-coating method renders surfaces with functional groups for further functionalization such as non-fouling surfaces. However, this pre-coating step results in an uneven coating layer with a dark color and still needs additional post-modification steps to introduce bio-inert polymers onto the pre-coating layer. Thus, finding an easy-to-use, one-step, surface-independent non-fouling coating through the combination of catechol groups and hydrophilic polymers is highly desirable.

Zwitterionic PCB material distinguishes itself due to its superior hydration capability, stability, and potential for further functionalization. [6] A prototype of universal "graft-to" coating materials based on polysulfobetaine (pSB) and a catechol group was previously developed by our group. [7] However, non-fouling properties of PCB coatings on

hydrophobic surfaces proved difficult to achieve when using the same single catechol-polymer conjugation as pSB; we believe this to be attributed to the superior super-hydrophilic nature of PCB. While additional DOPAmine functionalization resulted in an increased coating performance against a single protein fouling test, it was still insufficient against 100% serum.[8]

Despite previous efforts for "graft-to" coatings, no systematic study has been able to explain, on a molecular-level, the structure–property relationship of PCB universal coatings. Thus, a fundamental understanding of the structure-property relationship is highly desired. Therefore, the objective of this work is to develop a universal surface-independent non-fouling PCB coating using a "graft-to" approach.

To achieve this objective, we first sought to understand the structure-property relationship between the structure of a coating material and its coating performance such that we will be able to achieve similar performance of "graft-from" methods using the "graft-to" method which is much simpler for surface modification. For "graft-to" coating methods, we believe that two factors are critical in the design of molecular structures: (i) binding strength and (ii) packing density. Strong binding strength ensures that the highly hydrophilic PCB polymer can firmly attach onto the surface which, in return, increases both coating performance and stability. High packing density is needed for optimal nonfouling performance but proves challenging due to the high molecular-weight of bio-inert polymers that subtend too large a free volume in aqueous solutions to be packed densely on the surface, leaving large empty spaces between molecules. On the contrary, low molecular-weight bio-inert polymers may not be sufficient to form a densely packed

layer. In this work, we aim to study these two parameters by manipulating the molecular structure of PCB and DOPA conjugates.

First, we investigated the effect of the number of DOPA binding groups on polymer conjugates to minimize dissociation from targeted surfaces. Thus, a series of zwitterionic polymer-catechol conjugates of $(PCB)_m$-$(DOPA)_n$ with only one linear PCB polymer chain (m=1) with DOPA groups (n=1, 2, 4) were prepared as seen in **Figure 2.1**.[9]

Second, inspired by the smaller hydrodynamic volume of star-shaped polymers compared to linear counterparts of the same molecular weight, we investigated the effect of PCB chain structure from linear to star-shaped. Here, as before, $(PCB)_m$-$(DOPA)_n$ conjugates of the same binding block (n=4), but different PCB structures (where linear m=1, and star-shaped n=4) were designed. It was expected that the reduced radius of gyration of PCB star-shaped polymers would expose binding groups, reducing the probability of trapped binding groups in the coating process, thus, creating a "Janus" form. This "Janus" form star-shaped conjugate (m=4, n=4) had a clear separation between the exposed bio-inert PCB "face" and the surface-binding DOPA "face". This lead us to further hypothesize that this star-shaped conjugate with a "Janus" form would have less steric hindrance between molecules on the surface than its linear conjugate counterpart, which would achieve a higher packing density as seen in **Figure 2.1**.[10] All of four $(PCB)_m$-$(DOPA)_n$ conjugates were controlled to possess a similar molecular weight by atom transfer radical polymerization (ATRP) so that coating performance is exclusively caused by the difference in their structures rather than molecular weights. This library of $(PCB)_m$-$(DOPA)_n$ conjugates with different molecular architectures (n=1, 2, 3 and m =1, 4) were designed and synthesized using the concept of modular synthesis. Then, the efficiencies of different

molecules coated on commonly used biomaterial surfaces were quantitatively compared using an enzyme-linked immuno sorbent assay (ELISA) and *Staphylococcus Aureus* bacteria attachment test. Then, surface plasmon resonance (SPR) was used as it is a powerful technique to measure the interactions between biomolecules and surfaces with high sensitivity (0.3 ng/cm^2); we modified SPR chips with hydrophobic hydrocarbon self-assembled monolayers (SAMs) to mimic commonly used polymeric surfaces. The difference on fouling prevention against undiluted human serum due to their molecular structures can be quantitatively measured from SPR experiments. A fundamental understanding of how molecular architecture affects non-fouling performance will not only guide the development of effective coatings, but also shed lights on the general principles of "graft-to" coatings.

.

2.2 Experimental Section

2.2.1 Materials

CB-tBu monomer was synthesized according to a previously reported protocol.[15] The following chemicals and materials were purchased from Sigma-Aldrich (St. Louis, MO, USA), and were used as received: Anti-fibrinogen antibody produced in goat (anti-fibrinogen), triethylamine (TEA, 99%), N,N-diisopropylethylamine (DIPEA, 99.8%), 1-decanethiol (96%), α-bromoisobutyryl bromide (98%), Alexa Fluor 568 tagged bovine serum albumin, and Alexa Fluor 488, copper (I) bromide (CuBr, 98%), N,N,N',N'',N''-pentamethyldiethylenetriamine (99%), tetrabutylammonium fluoride hydrate (TBAF, 98%), trifluoroacetic acid (TFA, 99%), methanol (99.9%), bovine plasma fibrinogen, phosphate-buffered saline (PBS, 0.01 M phosphate) package, and Whatman 1 filter paper.

α-Bromoisobutyryl bromide (BIBB) N,N'-dicyclohexylcarbodiimide (DCC, 99.8%), ethylene glycol (99.8%), sodium azide (NaN_3, 99%), trifluoromethanesulfonic acid (TfOH, 99%), sodium carbonate (99%), N, N'- diisopropylcarbodiimide (DIPC, 99%), 4-dimethylaminopyridine (DMAP, ≥99%), 4-pentynoic acid (98%), 1-thioglycerol (98%), bovine serum albumin (96%), o-phenylenediamine (OPD, 98%), N,N-dimethylformamide (anhydrous 99.8%). o-phenylenediamine (OPD, 98%). The following chemicals and materials were purchased from Thermo Fisher Scientific (Waltham, MA, USA), and were used as received: dichloromethane (DCM, Reagent grade), hexanes (Certified ACS), tetrahydrofuran (THF,) toluene (ACS grade), methanol (Reagent grade), N,N-dimethylformamide (anhydrous 99.8%, Sigma-Aldrich), acetone (Certified ACS). Pooled human blood serum was purchased from BioChemed Services (Winchester, VA, USA). Ethanol (200 proof) was purchased from Decon Labs. Polydimethylsiloxane (PDMS; Sylgard 184) was purchased from Dow Corning. The water used in these experiments was obtained from a Millipore water purification system with a minimum resistivity of 18.0 MΩ cm. Bovine serum albumin (96%), High-impact PS, PVC, PP were purchased from Tapplastics.

2.2.2 Synthesis of $(PCB)_m$-$(DOPA)_n$ conjugates:

Initiator synthesis is described in detail in supporting information. Initiator (0.02 mmol), CB-tBU (1632mg, 6 mmol), CuBr (5.74 mg, 0.04 mmol) and methanol (3 mL) were added into a 100 mL Schlenk flask equipped with a stirring bar. The mixture was degassed by three freeze-pump-thaw cycles before the addition of PMDETA (13.87mg, 0.08 mmol). The reaction mixture was stirred at room temperature for 24 hours. After the reaction reached a desired conversion, the solution was directly transferred onto a 3.5k

dialysis bag and dialyzed against DI water for 48 hours to remove unreacted monomer and copper complex. The product was obtained as a white solid (PCB-$(DOPA)_4$-BOC-TBDMS) after freeze-drying for 24 hours. TBDMS and BOC removal of PCB-$(DOPA)_4$: To a 50 mL round bottom flask equipped with a stirring bar was added PCB-$(DOPA)_4$-BOC-TBDMS (550 mg, 0.02 mmol) and 3ml 3M methanolic HCl. The solution was stirred at room temperature for 3 hours. The solution was blown dry under nitrogen overnight and dissolved in 3ml of methanol. The polymer was obtained after precipitation in diethyl ether and centrifugation at 4200rpm for 2 minutes. The product was obtained as insoluble white solid.

2.2.3 Surface Coating on Samples:

6 mg PCB-DOPA polymer was dissolved in 0.6 ml of methanol and followed by adding 3 mL Tris buffer (pH=8.5) in a 5 mL centrifuge tube. The testing surfaces (0.6cm x 0.8cm) were washed sequentially with ethanol and water for 3 times and blown dry with airflow. Afterward, all testing surfaces were placed into the tube and submerged for 24 h. The testing surfaces after coating was washed with DI water twice and dried with airflow before the test.

2.2.4 SPR Measurement of 100% Serum fouling:

**The SPR sensor chips were prepared and cleaned as reported.[2b] The SAMs of 1-decanethiol were formed by immersing SPR sensor chip in the ethanol solution of 1-decanethiol (0.2 mM) for 24 h. The chips were then removed and washed thoroughly with ethanol and then dried with stream of air. The SAMs covered SPR chips were coated with

PCB conjugates as describe above. A custom-built SPR sensor from the Institute of Photonics and Electronics, Academy Sciences (Prague, Czech Republic) was used in this study. This experiment follows the sequence of flowing PBS for 10 min, undiluted serum for 10min, and then PBS for 10 min at flow rate of 40 μL/min. For the SPR sensor used in the study, a 1-nm SPR wavelength shift represents a surface coverage of ~17 ng/cm^2 for proteins. Detection limit for the SPR sensor used in this work is 0.3 ng/cm^2.

2.2.5 *Bacteria Adhesion:*

A gram positive strain of S. aureus was incubated in trypticase soy broth (TSB) for 12 h at 37 °C with shaking at 200 rpm. The suspended culture was diluted and then additionally grown in TSB for 2 h to reach exponential growth phase. When the second suspended culture reached an optical density of 1.0 at 600 nm, bacteria were centrifuged at 8000 rpm and suspended in sterile PBS (pH 7.4) buffer to a concentration of about 1 × 108 CFU mL-1. Different testing surfaces were cut in to 1cm^2 squares (1cm x 1cm) and then placed in the bacteria wells and followed by 24h incubation at 37°C. Afterward, all wells were gently washed with sterile PBS (pH 7.4) buffer to remove non-adherent bacteria and then stained with 0.5m SYTO9. The results were directly observed using both Nikon Eclipse TE2000-U and Nikon Eclipse 80i microscopes. The numbers of bacteria adhered on the surfaces were determined from images taken from three specimens of each sample. Data were normalized to that of TCPS sample.

2.3 Results and Discussion

2.3.1 *Synthesis and Characterization*

A library of molecules was synthesized individually. In order to simplify this process and avoid complicated architectures and synthesis, we introduced a novel concept of "modular synthesis". In a modular design, target molecules are referred to as building blocks that are synthesized individually.[11] Then each building block can be linked via selective and orthogonal CuAAC "click" chemistry philosophies to yield the desired targeted molecule.[12] In this case, we divided the types of molecules into three parts: (1) DOPA binding blocks, (2) dendritic linkers and (3) initiation blocks. (1) DOPA binding blocks function as universal surface-independent binding site; the addition of each (e.g. n= 1, 2, 4) binding sites is expected to exponentially increase binding strength by an order of magnitude. (2) Dendritic linkers control the number ratio between DOPA binding blocks and initiation blocks. (3) Initiation blocks control the structure of zwitterionic polymer chains (linear or star-shaped). All blocks were synthesized respectively and linked by orthogonal copper(I)-catalyzed alkyne-azide cycloaddition (CuAAC) "click" chemistry to ensure the structure integrity of building blocks as shown in **Scheme 1**. Unlike conventional amphiphilic block copolymers, these modular designed structures can achieve precise structure control and clearly separate the binding groups and the polymer chain.

To initiate synthesis, DOPA binding block **1** was prepared from the protection of DOPA with t-butyldimethylsiloxy (TBDMS) and di-tert-butyl dicarbonate (BOC). Dendritic linkers **2** and **3** were prepared by an step esterifications between α-Bromoisobutyryl bromide (BIBB) and 2-bis(oxymethyl)- propionic acid, following the previously reported procedure to give well controlled dendritic linkage sites.[11c] The protected DOPA block was then coupled with linkers **2** and **3** to afford an 85% yield of the 1Br-2DOPA **5** and 65%

yield of the 1Br-4DOPA **6**, respectively. Similarly, the multi-head initiation block was prepared by the same step growth methodology from 3-butyn-1-ol to the second dendron linker **7** with 75% yield. The BIBB was again coupled to the four hydroxyl groups on dendron linker **7** in DCM in the presence of DMAP to afford a 95% yield of the 1Alkyne-4Br **8**. The substitution of Br groups on **6** with sodium azide was carried in DMF solution with 5 equiv. of sodium azide, affording a 95% yield of the $1N_3$-4DOPA. The nucleophilic substitution reaction using the existing initiator **6** significantly simplified the synthesis route. The high efficiency of CuAAC "click" between **8** and $1N_3$-4DOPA gives 4Br-4DOPA (initiator **9)** with 85% yield (Scheme 1). The structure correctness of each building block was characterized by nuclear magnetic resonance (NMR) (**Figure 2.2**a, b, c, d) and confirmed by time of flight mass spectroscopy (TOF-MS)

2-tert-butoxy-N-(2-(methacryloyloxy)ethyl)-N,N-dimethyl-2-oxoethanaminium (CB-tBu) was chosen as a monomer for its excellent compatibility in this polymerization system. The tert-butyl protection can also be easily removed under acidic conditions. The polymerization of CB-tBu monomer was carried out in methanol solution at room temperature for 24 hours using Schlenk techniques (**Scheme 2.2**). Hydroxyl groups in the catechol were protected by TBDMS since the catechol functions as an inhibitor in radical polymerization. Degree of polymerization was controlled at 50% to give a narrow molecular weight distribution. Gel permeation chromatogram (GPC) analysis indicated that all the polymers prepared through ATRP had symmetric mono-model distributions and very close molecular weights **(Figure 2.2e).** The comparable molecular weight ensures the fair comparison of how molecular structure affects performance. Degree of polymerization was quantitatively calculated by NMR integration data (**Table 2.1**). As shown in Scheme

2, all protection groups (TBDMS, Boc and tert butyl) were removed simultaneously in 3M methanolic HCl for 5 hours. NMR spectrum confirmed the high efficiency of the deprotection reaction **(Figure 2.2f, g).**

2.3.2 *Surface Characterization:*

Figure 3a summarizes the contact angle results of all commonly used materials (glass, polydimethylsiloxane (PDMS), polystyrene (PS) and polypropylene (PP)), before and after coating. All surfaces coated with $(PCB)_4$-$(DOPA)_4$ resulted in a significant decrease in contact angle to 14±1 degree. No observable difference was observed between different molecules due to the limited sensitivity of this technique.

The formation of a uniform and homogeneous coating layer was confirmed by atomic force microscopy (AFM). **Figure 2.3b** shows a typical 3D surface morphology of PDMS substrate after being coated with $(PCB)_4$-$(DOPA)_4$ conjugates. AFM results indicated that the roughness of PCB coated PDMS surface is around 2 nm at the dry state, which corresponds well with that of the unmodified PDMS surface. The smooth surface demonstrates the high uniformity of the polymer coating, which is critical in reducing the attachment of biofoulants.

2.3.3 *ELISA Measurements of Protein Adsorption*

Several commonly used materials in biomedical devices were tested for their coating performance in this study. Hydrophobic PP and PDMS are commonly used as artificial organ materials while polyvinyl chloride (PVC) and PS are often used as blood contacting

tubing.[1c] It is also worth noting that among these polymeric materials, PDMS and PVC were chosen due to their difficultly in being treated by "graft-to" methods. This is due to (1) the PDMS low surface energy and active reconstruction, and, (2) the PVC surface leachable thin layer (plasticizer covering the entire surface); thus, to overcome all these shortcomings, it requires polymer coatings that have very strong binding groups to achieve surface attachment.[13] Coating performance of $(PCB)_m$-$(DOPA)_n$ conjugates on each material was tested using ELISA experiments as reported.[8, 14] o-phenylenediamine dihydrochloride (OPD) in 0.1 M citrate phosphate buffer induced a chromogenic reaction in anti-human plasma HRP-Fibrinogen conjugate protein; the resulting UV absorbance at 492nm was recorded for a visualized comparison among conjugates. Here, the intensity of the tangerine color of the solution was proportional to the amount of nonspecific adsorbed proteins. For quantitative comparison, fouling results on the uncoated bare surfaces were normalized to 100%.

As shown in **Figure 2.3c**, generally all $(PCB)_m$-$(DOPA)_n$ conjugates showed reduction in protein adsorption on all the surfaces. For $(PCB)_1$-$(DOPA)_1$ conjugate with only one polymer chain and one DOPA binding site, we observed reduction in the fouling level. A reduction of nonspecific protein fouling to 18.5%, 12.9%，22.7%, 17.5%, 30.10% was observed on PP, PVC, PS, PDMS and glass surfaces, respectively after these surfaces were soaked in $(PCB)_1$-$(DOPA)_1$ Tris solution. This indicated that a zwitterionic polymer layer can be introduced onto these surfaces, reducing nonspecific adsorption of single protein up to a certain extent. When the binding sites were expanded into two while maintaining the same molecular weight of PCB, as $(PCB)_1$-$(DOPA)_2$, fouling levels were further decreased to 3.1%， 5.4%， 5.4%， 7.4%, and 17.45% for PP, PVC, PS, PDMS and glass,

respectively. When DOPA binding sites were even expanded into four, a further decrease in the fouling level, although not significant, can be observed after the treatment of $(PCB)_1$-$(DOPA)_4$, which are 2.3%，3.9%，4.1%, 5.9% and 10.4% for PP, PVC, PS, PDMS and glass, respectively. The identical trend observed on all these surfaces confirmed that monovalent binding group is not enough to counterbalance the strong hydration force between PCB and water molecules. Thus, multivalent binding groups should be properly introduced to polymer conjugates to increase binding strength and achieve high coating coverage toward targeted surfaces. From ELISA testing, $(PCB)_1$-$(DOPA)_1$ polymer reduced fouling to roughly below 20%. After introduction of one more pair of DOPA binding group, $(PCB)_1$-$(DOPA)_2$ brought the fouling level to lower than 10%, which indicates that an additional binding site can significantly improve the binding affinity of conjugates onto the surface. A further decrease in fouling level below 5% was achieved by the tetravalent $(PCB)_1$-$(DOPA)_4$ conjugates. A stable coating with high surface coverage was achieved only by the addition of a strong binding force that could outweigh the peeling strength of water molecules. The enhanced performance with increasing number of DOPA binding groups is due to the increased surface binding strength and decreased dissociation of polymers from the surface **(Figure 2.1).** In addition to the number of binding sites, performance can be further improved by adjusting polymer structures. For the coating using $(PCB)_4$-$(DOPA)_4$, a slight decrease in fouling to 1.7%, 1.9%, 2.4%, 4.3% and 6.2% was observed for PP, PVC, PS, PDMS and glass, respectively. In this case, a star-shaped polymer chain outperformed its linear counterpart $(PCB)_1$-$(DOPA)_4$ on coating performance since star-shaped polymer chain can reduce steric hindrance between molecules, thus achieving high surface packing density. However, ELISA data for $(PCB)_4$-

$(DOPA)_4$ and $(PCB)_1$-$(DOPA)_4$ are all below 5% for a single protein solution test. In order to distinguish their difference quantitatively, further characterization was performed with a highly sensitive SPR for protein adsorption against 100% human serum.

2.3.4 *SPR Measurement of Protein Adsorption from 100% Serum*

The real-time protein adsorption was measured with a custom-built SPR sensor from the Institute of Photonics and Electronics, Academy Sciences (Prague, Czech Republic). For the SPR sensor used in this study, a 1 nm SPR wavelength shift at 750 nm between two buffer baselines before and after serum injection represented a surface coverage of 15 ng/cm^2 adsorbed proteins on the surface. The detection limit of the SPR sensor used in this work was 0.3 ng/cm^2. To quantitatively evaluate the influence of structure on non-fouling ability of PCB coating, hydrocarbon SAMs on a gold chips were coated with all four $(PCB)_m$-$(DOPA)_n$ conjugates. Hydrocarbon SAMs were chosen to mimic hydrophobic polymeric surfaces. Due to the ability of DOPA to bind much better for hydrophilic surfaces than hydrophobic surfaces, only hydrophobic surfaces are studied here. All samples flowed with PBS buffer for 10 min, followed by 100% blood serum at a flow rate of 40 mL/min for 10 min, and then washed by PBS buffer for 10 min. (**Figure 2.3d**).

Figure 2.3d shows the change in the SPR signal attributed to protein adsorption from serum as a function of time on a hydrophobic SAM coated with four zwitterionic polymer-DOPA conjugates. The wavelength shifts in the $(PCB)_1$-$(DOPA)_1$ and $(PCB)_1$-$(DOPA)_2$ treated hydrophobic surfaces were 5nm and 3.2nm, respectively, corresponding to the

adsorbed protein level of 75ng/cm^2 and 48ng/cm^2. These results correspond well with those observed on fouling tests using single protein showing that stronger surface binding is critical. Doubling the binding sites to four decreased protein adsorption levels further to 33.15ng/cm^2 (2.21nm) for $(PCB)_1$-$(DOPA)_4$ treated hydrophobic surfaces. As a control, uncoated hydrophobic SAM surface had a protein adsorption of 260 ng/ cm^2 after the flow of 100% human serum. It is also worth noting that for all surfaces treated with star-shaped chain conjugates $(PCB)_4$-$(DOPA)_4$, the wavelength shifts were consistently the lowest (only 1.3nm) with a protein adsorption of 19.5ng/cm^2.

SPR and ELISA experiments for linear conjugates (n=1, m=1,2,4) showed decreasing fouling level trends with increasing DOPA binding blocks. There is an equilibrium of conjugates between the surface and the solution when surface binding force is not strong enough (e.g., n=1) to overcome the dissociation force of PCB polymer from the surface to the solution due to the high solubility of PCB polymers. The increasing of binding groups (e.g., n=2 or 4) can significantly improve the adhesion of PCB polymers onto the target surface.

From $(PCB)_1$-$(DOPA)_4$ and $(PCB)_4$-$(DOPA)_4$, it can be seen that the star-shaped polymer (m=4) exhibited a 0.58-fold lower protein adsorption than linear counterparts (m=1) against undiluted human serum despite both molecules exhibiting the same binding strength (n=4). This difference can be explained by two possible structural reasons: (a) exposure of the anchor group and (b) steric hindrance. First, the multi-arm star-shaped polymer has a shorter chain length at each arm than the linear one, resulting in a more confined, stiffer conformation on each chain **(Figure 2.1).** These four arms are confined to

one side while the tetravalent binding group is well exposed to the other side. The conjugate of the "Janus" form is more favorable in its self-assembly onto a surface. On the contrary, a linear polymer chain has a high chance to trap its anchoring groups due to its high flexibility, reducing the chance of its surface attachment. Second, the steric interactions of adsorbed molecules on the surface are another dominant factor in achieving a high packing density. Since the radius of gyration of a star-shaped polymer is smaller than that of its linear polymer counterpart with the same degree of polymerization, polymer with the star-shaped structure is able to make the bio-inert "face" of this "Janus" form conjugateless bulky than the linear structure. This feature is favorable to a dense pack on the surface, leading to a higher surface coverage **(Figure 2.1).**

2.3.5 *Stability*

Long-term stability of coatings were investigated for all substrates: PP, PS, PDMS, and PVC. Here, all substrates were treated with $(PCB)_4$-$(DOPA)_4$. Then, they were stored in PBS buffer for two weeks and tested by ELISA. No notable change in fouling level was observed after storage for 1, 7, and 14 days. This result further gives evidence that stronger binding forces, obtained by using multi-binding sites, not only increases anti-fouling capability, but also coating life span **(Figure 2.3e).**

2.3.6 *Bacterial Attachment*

A gram-positive strain of *Staphylococcus Aureus* was used to examine bacteria attachment on coating surfaces. Shown in **Figure 2.4**, coated surfaces resulted in a significant reduction in bacterial attachment compared to the non-coated control. Results show $(PCB)_4$-$(DOPA)_4$ coated surfaces exhibited the lowest bacterial attachment for all tested

coated substrates and minimal bacterial attachement for $(PCB)_1$-$(DOPA)_1$ coated surfaces. This trend was identical in performance for coatings with both bacteria and protein fouling results. Thus, this suggests $(PCB)_4$-$(DOPA)_4$ coated surfaces yields better results due to strong surface binding from more DOPA binding units, and, thus, suggesting that higher surface coverage serves as the critical issue for "graft-to" coatings.

2.4 Conclusions

In summary, we found the optimal coating for long-term stability performance using a "graft-to" method had the highest amount of binding DOPA sites. Four types of zwitterionic polymer-catechol conjugates of precisely controlled structures were synthesized. Their non-fouling properties were verified via ELISA and SPR. By comparing a single-binding group of $(PCB)_1$-$(DOPA)_1$ to multivalent-binding groups of $(PCB)_1$-$(DOPA)_2$ and $(PCB)_1$-$(DOPA)_4$, we were able to significantly increase the binding affinity of PCB polymer on varying target surfaces. Even more, by adopting a star-shaped chain structure of $(PCB)_4$-$(DOPA)_4$, we were able to reduce steric hindrance between conjugates, and therefore expose more binding groups. This combination of a star-shaped chain structure with multiple DOPA binding groups created a clear separation between the outer bio-inert polymer and its inner binding blocks layer, thus, forming a "Janus" form conjugate, which in return increased the packing density independent of targeted surfaces. Thus, the $(PCB)_4$-$(DOPA)_4$ conjugate resulted in the most effective structure in terms of stable long-term attachment regardless of targeted surfaces under physiological conditions for at least 2 weeks. The SPR tests showed that the "Janus" form, $(PCB)_4$-$(DOPA)_4$ coating on hydrophobic SAM, yielded a protein adsorption of 19.5 ng/cm^2 in 100% human serum. With its superior stability, this is the best result of surface–independent "graft-to"

zwitterionic coating reported to our knowledge, thus, demonstrating that using the design principle of the "Janus" form proves as a useful guide to achieving high performance "graft-to" coating molecules.

2.5 Tables

Table 2.1. Characters of $(PCB)_m$-$(DOPA)_n$ conjugates

pCB-DOPA conjugates	Number of polymer arms	Polymer architecture	Total Mw of pCB	Total degree of polymerization	Number of DOPA blocks	Total molecular weight	PDI
$(pCB)_1$-$(Dopa)_1$	1	Linear	38270	178	1	38660[a)]	1.06
$(pCB)_1$-$(Dopa)_2$	1	Linear	33325	155	2	34009	1.05
$(pCB)_1$-$(Dopa)_4$	1	Linear	36500	170	4	37776	1.04
$(pCB)_4$-$(Dopa)_4$	4	Star-shaped	35260	164	4	37512	1.06

a)Molecular weight of polymers was calculated by NMR integration.

2.6 Figures

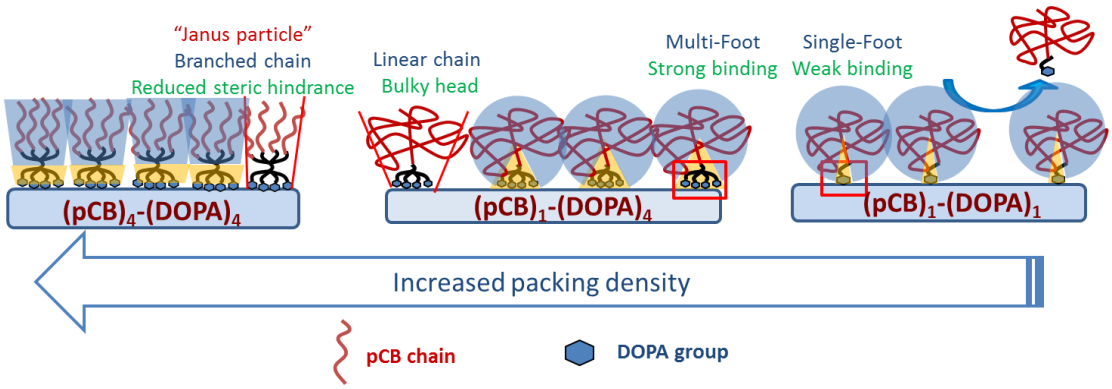

Figure 2.1. Scheme of the structural and binding effects of $(PCB)_m$-$(DOPA)_n$ conjugates.

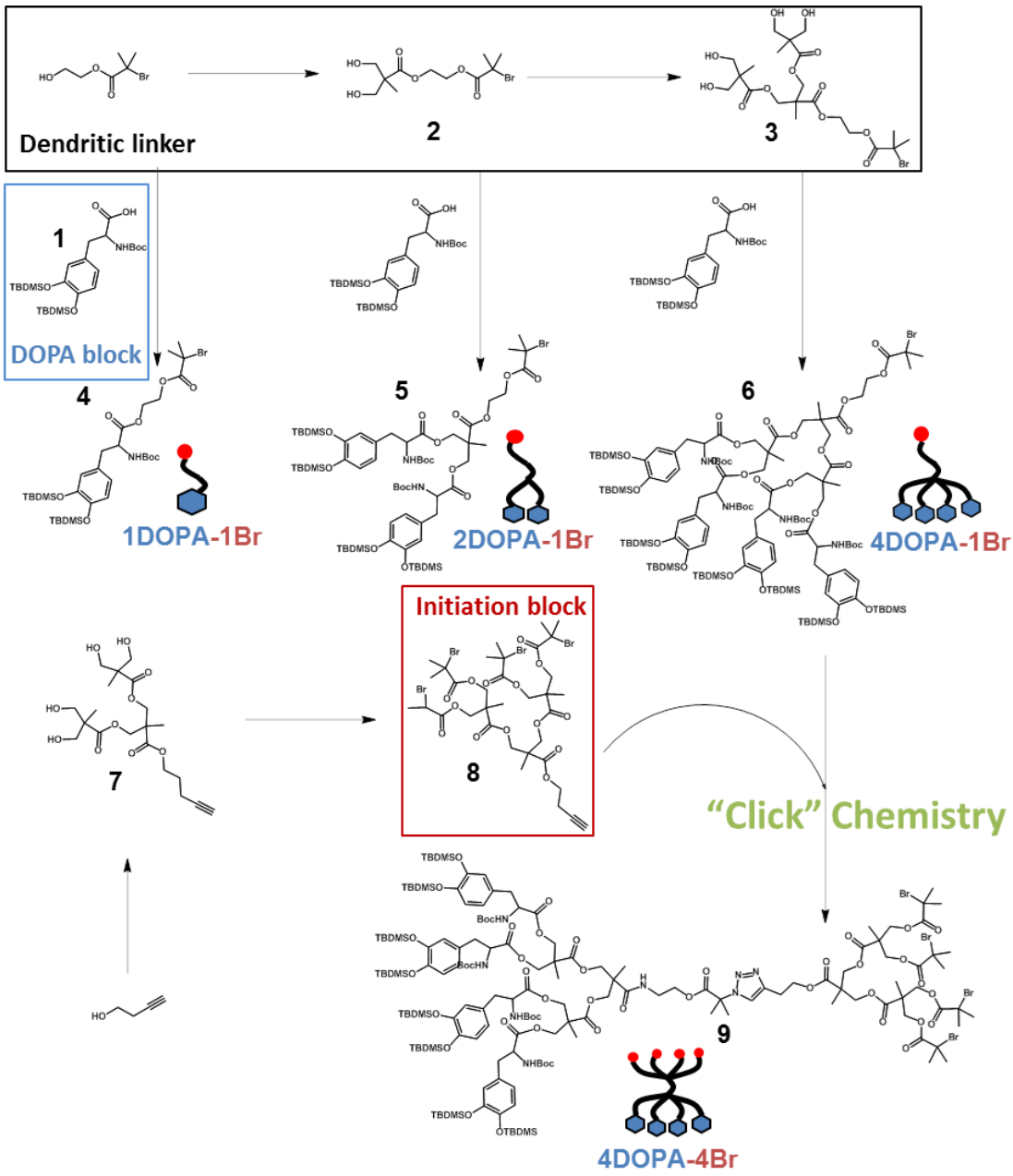

Scheme 2.1. Synthesis of initiators

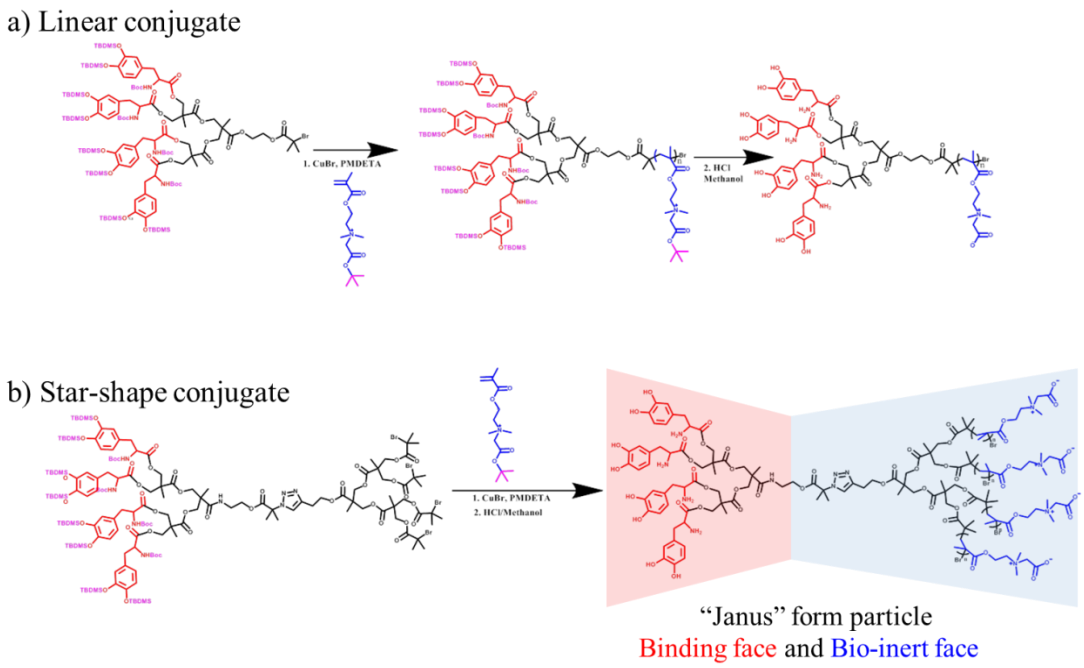

Scheme 2.2. Synthesis of a) linear conjugate $(PCB)_1$-$(DOPA)_4$. b) "Janus" form star-shaped conjugate $(PCB)_4$-$(DOPA)_4$. Other conjugates follow the same scheme using different initiators. Conjugates are composed of DOPA binding block (red), dendritic linker (black), and bio-inert polymer block (blue).

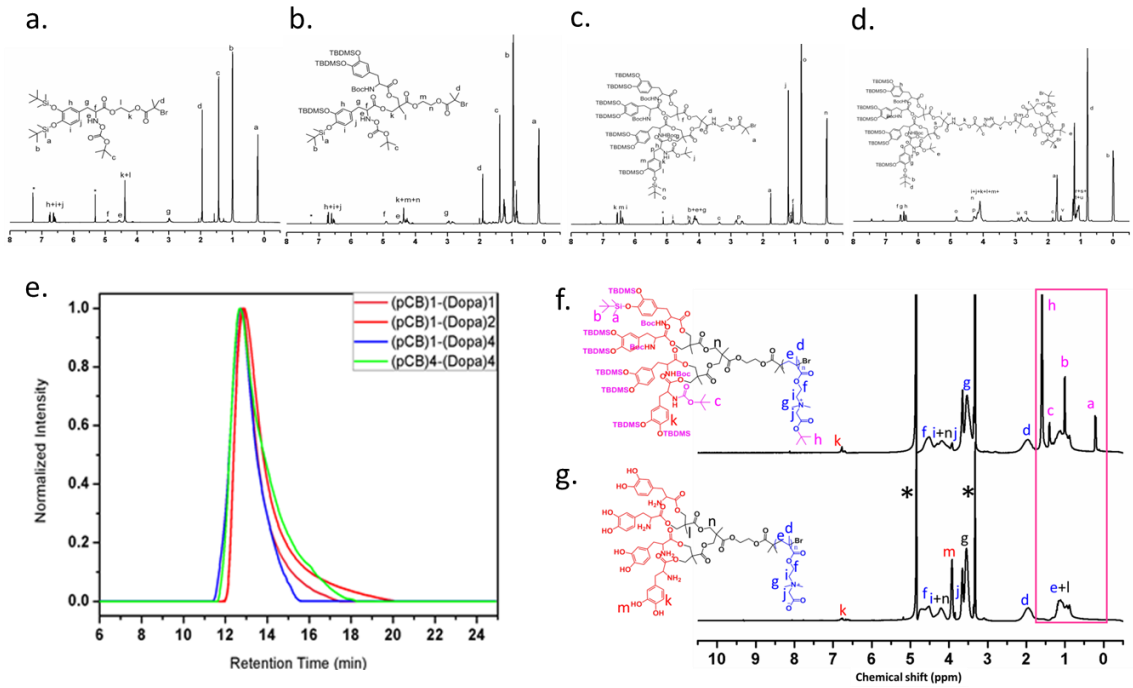

Figure 2.2. NMR spectrums of synthesized initiators： a) 1DOPA-1Br. b) 2DOPA-1Br. c) 4DOPA-1Br. d) 4DOPA-4Br. e) GPC data of $(PCB)_m$-$(DOPA)_n$ conjugates. f) $(PCB)_1$-$(DOPA)_4$ conjugate with protection groups (pink). g) $(PCB)_1$-$(DOPA)_4$ conjugate after deprotection.

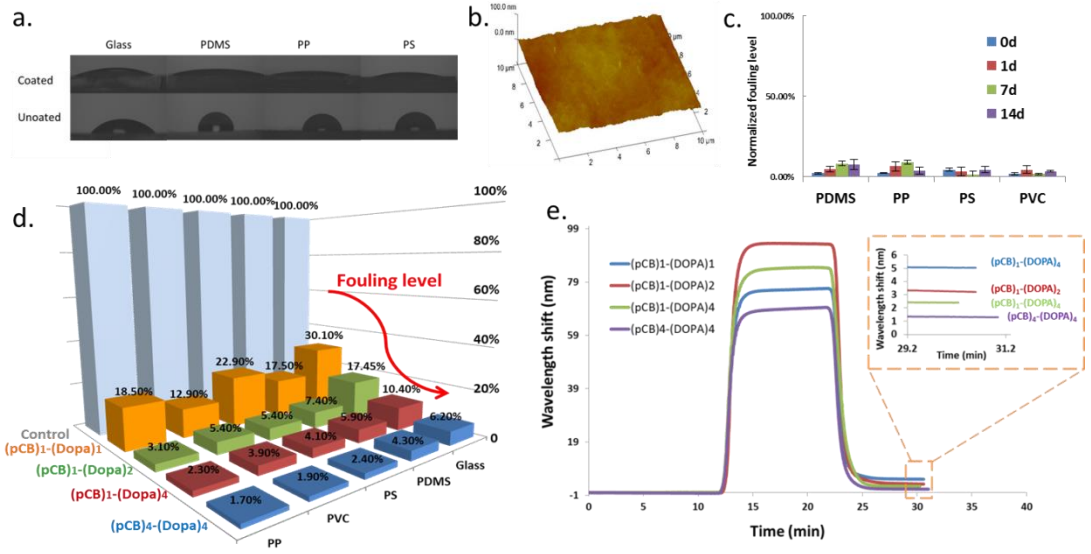

Figure 2.3. a) Contact angle of pure water on uncoated and $(PCB)_4$-$(DOPA)_4$ coated surfaces. b) AFM 3D imaging of a $(PCB)_4$-$(DOPA)_4$ coated PDMS surface. c) Protein adsorption of $(PCB)_4$-$(DOPA)_4$ modified surfaces after stored in PBS buffer for 1, 7 and 14 days. d) Protein adsorption on PS, PP, PDMS and PVC surface before and after $(PCB)_m$-$(DOPA)_n$ treatments. e) SPR sensorgrams of non-specific protein adsorptions of $(PCB)_m$-$(DOPA)_n$ coated 1-decanethiol SAMs on Au surfaces against 100% human blood serum.

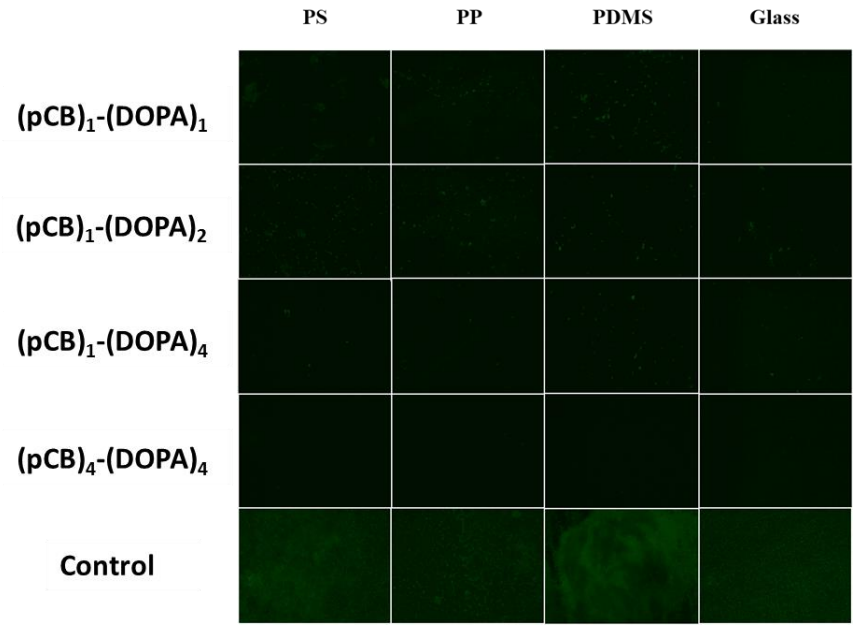

Figure 2.4. Bacteria attachment $(PCB)_m$-$(DOPA)_n$ on different surfaces

Chapter 3 *In vivo* sheep and rabbit models for evaluating low-fouling zwitterionic polymer coatings in artificial lungs

Current artificial lungs fail in [16-19] weeks due to surface-induced thrombosis. Biomaterial coatings may be applied to anticoagulate artificial surfaces, but none have shown marked long-term effectiveness. Poly-carboxybetaine (PCB) coatings have shown promising results in reducing protein and platelet-fouling *in vitro*. However, *in vivo* hemocompatibility remains to be investigated. Thus, two different PCB-grafting approaches to artificial lung surfaces were first investigated: 1) "graft-to" approach using 3,4-dihydroxyphenylalanine (DOPA) conjugated with PCB polymer (PCB-$(DOPA)_4$); 2) "graft-from" approach using the Activators ReGenerated by Electron Transfer method of atom transfer radical polymerization (ARGET-ATRP). One device coated with each of these methods and one uncoated device were attached in parallel within a veno-venous sheep extracorporeal circuit with no continuous anticoagulation (N=5 circuits). The PCB-(DOPA)4 approach showed the least increase in blood flow resistance and the lowest incidence of device failure over 36-hours. Next, we further investigated the impact of tip-to-tip PCB-(DOPA)4 coating in a 4-hour rabbit study with veno-venous micro-artificial lung circuit at a higher activated clotting time of 220-300s ($N \geq 5$). Here, PCB-(DOPA)4 reduced fibrin formation ($p=0.06$) and gross thrombus formation by 59% ($p<0.05$). Therefore, PCB-$(DOPA)_4$ is a promising material for improving the anticoagulation of artificial lungs

3.1 Introduction

Over 168,000 Americans die every year due to chronic respiratory diseases. [16-19] The only long-term treatment option is lung transplantation, but only 2345 lung transplants take place each year in the United States.5 Extracorporeal membrane oxygenation (ECMO) is an alternative means of long-term respiratory support which performs gas exchange using a densely-packed bed of hydrophobic hollow fibers. However, these fiber surfaces are especially susceptible to surface-induced coagulation, ultimately resulting in device failure within 1-4 weeks. [21-26] Currently, heparin is administered as an anticoagulant to prolong the device lifespan, but bleeding complications are prevalent and often fatal during ECMO.9,10 Hence, an alternative anticoagulation approach with minimal systemic effect would be highly desirable.

To reduce thrombosis only at blood-contacting surfaces, anticoagulant molecules such as heparin and low-fouling polymers such as polyethylene glycol (PEG) have been applied over oxygenator surfaces. However, the existing coating technology is not sufficient for extending the device's useful lifetime. Surface-bound heparin has reduced bioactivity compared to its soluble form,11 and several studies have reported no clear benefits of PEG coatings when in contact with in whole blood.[27,28]

Carboxybetaine (CB) on the other hand, is a newer class of low-fouling molecule that has shown promising in vitro results for repelling protein and platelet fouling. [25] CB is zwitterionic, defined as having both positive and negative charges while retaining a net neutral charge. The equal and opposite charges present on zwitterionic molecule electrostatically attract water molecules, forming a robust hydration layer that repels non-specific protein adsorption.18 Previous work has coated hydrophobic surfaces such as

poly-(dimethyl siloxane) (PDMS) and polypropylene (PP) with polycarboxybetaine (PCB) chains using both a "graft-to" approach via catechol groups like DOPA [27-28] or via multiple DOPAs and a "graft-from" approach using ARGET-ATRP. [16] These coated surfaces repelled non-specific protein adsorption and platelet adhesion efficiently even in complex media, including 100% plasma. However, several challenges exist for extending this to artificial lung applications. First, artificial lungs' gas exchange membrane surfaces are densely packed and complex in surface geometry. Additionally, an artificial lung circuit has multiple distinct types of synthetic polymer, which also raises the difficulty of achieving a uniform grafting across different surface characteristics. Finally, artificial lungs must repel non-specific protein adsorption under a rigorous, whole blood environment. Therefore, an ideal coating methodology specifically for artificial lungs must be determined, and its ability to impede clot formation must be evaluated in a clinically relevant model.

In the following studies, the optimal method of attaching PCB to the artificial lung surfaces was evaluated with two separate in vivo experiments. In the first, oxygenators with different PCB coating methods were attached in parallel in a 36-hour, sheep, veno-venous ECMO model. To achieve measurable clotting within the 36-hour time frame, sheep were not continuously anticoagulated. Under this rigorous whole blood environment, three different PCB attachment methods were compared. In each case, the goal was to develop a simple, flow-through coating method that would not significantly complicate the artificial lung construction process. The first coating used the "graft-to" method, in which direct surface attachment of PCB polymer chains was accomplished using the previously reported PCB-(DOPA)4 conjugate. [29-35] The second utilized a "graft-from" approach using

ARGET-ATRP. In the second in vivo study, the coating that exhibited the best thromboresistance was further investigated to determine its independent ability to slow clot formation when the entire circuit is coated using the same method. This study utilized a four-hour rabbit veno-venous extracorporeal circuit model with continuous anticoagulation to better reflect clinical environment.

.

3.2 Experimental Section

3.2.1 *Sheep Study*

Sheep Study, Miniature Artificial Lung Fabrication: Microporous PP fiber (Type X30-150, 3M, NC) was coated with thin polysiloxane layer (Applied Membrane Technology, MN). The siloxane-PP fiber was double-layered and knitted with a crossing angle of 30 degrees and fiber spacing of 43 fibers/inch. The mat was rolled into a fiber bundle with a path length of 1.5 cm. The bundle was then encapsulated in a PETG housing (McMaster-Carr, IL) and "potted" in place using PDMS (Elastosil RT 625, Wacker Chemie AG, Germany). Polyurethane filling (WC-575, BJB Enterprises, CA) was injected into the corner areas of the device at the cap-housing interface to reduce areas of stagnation and recirculation. Silicone tubing with inner diameter (ID) of 3/16" (McMaster-Carr, IL) was attached as blood inlet and outlet for the device. The completed device **(Figure 3.2a)** had a total fiber surface area of 0.1 m^2 and a frontal area of 14.5 cm^2. After fabrication, the device was coated with one of the three methodologies described below.

PCB Coating:

i) PCB-(DOPA)4 conjugate was synthesized using a method similar to one described previously,[19] but carboxybetaine methacrylate (CBMA) was used as the monomer instead of CBAA. This PCB-(DOPA)4 conjugate was then mixed in a water-methanol solution (80%/20% v/v) to achieve a concentration of 2 mg/mL, and 2-amino-2-hydroxymethyl-propane-1,3-diol (TRIS) salt was added to reach a pH of 8.5. The sample was incubated with this solution and then agitated for 20 hours.

ii) ARGET-ATRP PCB: The miniature artificial lung was completed filled with hydrogen peroxide/18.4 M sulfuric acid solution (30%/70% v/v) and then exposed for 60 seconds to hydroxylate the surfaces. Subsequently, the ARGET methodology followed our previously reported methodology.[30]

Sheep Study, Circuit Preparation: The miniature artificial lung was attached in a veno-venous, extracorporeal, parallel circuit configuration **(Figure 3.2b).** The 18-28 French dual lumen cannula (Avalon Elite, Maquet, NJ) provided both drainage and reinfusion. Tygon tubing was used for the circuit tubing material. The drainage cannula was followed by 220 cm of 3/8" ID tubing (Cole-Parmer, IL), followed by 75 cm of ¼" ID tubing (Saint-Gobain, France), which then fed into the portion of the circuit containing four artificial lungs in-parallel. Before entering the parallel lungs, blood flow from the cannula was divided into four separate branches using a 1/4"- 1/4" polycarbonate Y connector (Qosina, NY), followed by 10 cm of 1/4" ID tubing, and then another 1/4"-1/4" polycarbonate Y connector. After the second Y connector, each branch contained, in order: 6.5 cm of ID 1/4" tubing; 1/4"-3/16" polycarbonate reducer (Qosina, NY); 5 cm of ID 3/16" tubing

(Saint-Gobain, Courbevoie, France); 3/16”-3/16” polycarbonate luer connector (Qosina, NY); miniature artificial lung; 3/16”-3/16” polycarbonate luer connector; 5 cm of ID 3/16” tubing; 1/4”-3/16” polycarbonate reducer; 6.5 cm of ID 1/4” tubing. Four separate branches converged back to one flow using the same set of Y connectors as before for diverging the flow, but in a reverse order. Finally, 200 cm of 1/4” ID tubing, followed by 40 cm of 3/8” ID tubing, were used to direct the flow back to dual lumen cannula for reinfusion.

Sheep Study, Surgery: Two Montadale sheep were used for this study. Transdermal fentanyl patches (Apotext Corp, FL, 75 μg/hr) were applied to the sheep 12 hours before the surgery, and anesthesia was induced via intravenous injection of 4-6 mg/kg propofol (Fresenius Kabi, Germany). During the surgery, the sheep was ventilated with 100% oxygen mixed with 1-5 % isoflurane. The arterial line was placed in the carotid artery to obtain blood samples and mean arterial pressure (MAP) measurements. The dual lumen ECMO cannula was placed via the jugular vein and tunneled to the right atrium for drainage and reinfusion for the extracorporeal circuit. At initial attachment, the circuit was primed with saline containing 5000 units of heparin (Sagent, IL) and 30 mg/kg of methylprednisolone sodium succinate (Pfizer, NY). The initial attachment circuit did not include artificial lungs. Instead, the first device attachment was offset by at least 6 hours after the surgery, following the attachment protocol

The roller pump (COBE, CO) was used to achieve a total blood flow rate of 800 mL/min through the cannula and 200 ± 20 mL/min per branch. After the attachment surgery, the sheep was moved to a custom-built stanchion cage. Once the sheep was awake and alert post-surgery, it was transported to the animal facility for chronic monitoring and artificial lung attachment.

Sheep Study, Artificial Lung Attachment and Detachment: The first set of attachment was performed at least 6 hours after the surgery. Moreover, the devices were primed with normal saline at least 6 hours before the attachment to ensure that surfaces were sufficiently wetted. Prior to attachment, sheep was given an IV bolus of 50 units heparin/kg. The devices were attached two at a time using the following protocol. First, the total blood flow was reduced from 800 to 400 mL/min. Next, the circuit was clamped off after the first Y connector and right before the last Y connector to cut off blood flow from half of the circuit. The clamped-off section was removed and replaced with a primed device circuit containing two artificial lungs. The clamps were removed, and the flow was returned to 800 mL/min and adjusted further by placing adjustable clamps on each branch to ensure even distribution between the four branches. Once the flow through each device was at 200 ± 20 mL/min, initial baseline resistance measurement was recorded. After the baseline measurements were taken for both devices, the same set of procedure was followed for initial attachment of other two branches/devices.

Each artificial lung was detached from the main circuit 36 hours after attachment or when it met the failure criteria defined as follows: two consecutive resistance measurements were 100% greater than the initial, baseline resistance value. Prior to detachment, sheep were given an intravenous bolus of heparin (50 units/kg). The total blood flow was reduced to 200 mL/min per remaining device prior to device removal. After detachment, a piece of 3/16” ID Tygon tubing was put in the place of the removed lung. To keep the flow equal between all four branches, a Hoffman clamp was placed distal to each device outlet and adjusted accordingly. Each removed circuit was rinsed with a bolus of heparin (10,000

units) followed by heparinized saline (2 units/mL) until the effluent became colorless. Afterwards, the device was fixed with 2% glutaraldehyde (Electron Microscopy Sciences, PA) in phosphate buffer.

After all the devices from the first set were removed, a new set of devices was re-attached up to two more times afterwards if platelet count was at least 2/3rds of the baseline value. All devices were primed with saline for at least 6 hours prior to attachment to ensure that the surfaces were hydrated. Prior to re-attachment, sheep were given a bolus of 50 units/kg of heparin. After a maximum of 3 sets of devices, each sheep was given 0.22 mL/kg of sodium pentobarbital (Vortech Pharmaceuticals Ltd, MI) intravenously for euthanasia.

Sheep Management: During monitoring, the sheep was given either an intravenous drip of either saline or Lactated Ringer's solution at 1.2-5 mL/kg/hr. There was no continuous administration of anticoagulants in order to accelerate coagulation for this experiment. The fentanyl dermal patch was started 12 hours prior to the surgery and maintained for 72 hours. After the patch wore off, the sheep was given an intramuscular injection of 0.005-0.01 mg/kg buprenorphine every 4-8 hours (Renckitt Benckiser Pharmaceuticals, England). For antibiotics, 5 mg/kg enrofloxacin (Bayer, Germany) was given intravenously once a day, and 40,000 units/kg of procaine penicillin G/benzathine penicillin G combination (Aspen Veterinary Resources, MO) was given intramuscularly every 72 hours. The animal's arterial blood samples were taken to measure activated clotting time (ACT), hematocrit, and arterial blood gas (ABG) as needed or every 6 hours. Platelet and white blood cell counts were taken twice a day and plasma-free hemoglobin once a day.

Sheep Study, Digital Data: Mean arterial pressure was measured with patient monitor (Tram-rac 4A with Tram 600SL module, GE Marquette Electronics, WI). Device inlet and outlet pressures for each coating type were measured using Transpac transducers (ICU Medical Inc, CA). Flow rate was monitored using ultrasonic flow probe and flow meter (TS410 with 14PXL, NY). Both sets of measurements were recorded onto the monitoring computer using data acquisition system (Biopac Systems, CA). Blood flow resistance was calculated as: (inlet pressure – outlet pressure)/device flow rate.

Sheep Study, Data Processing and Statistical Analysis: The resistance measurements were log-transformed. For all statistical tests with repeated measures, a mixed linear model was used with animal subject and/or device number as the subject variables, time as the repeated measure, coating and time as fixed effects, and Autoregressive(1) as the repeated covariance matrix. Bonferroni correction was used for post-hoc correction for all pairwise comparisons. For devices that failed before the 36-hour time limit, the last recorded resistance measurement was kept until the 36-hour mark as a conservative estimate of the resistance had it been left attached. The Kaplan-Meier method was performed to compare device failure rates, using log rank as the statistical test for significant difference in failure rate. A p-value < 0.05 was considered statistical significance for all tests. The error bars in the figures represent standard error of the mean (S.E.M.) unless stated otherwise.

3.2.3. *Rabbit Study*

Rabbit Study, Micro Artificial Lung Fabrication: The same PDMS-PP fiber from the sheep study was used for these devices. The double-layered hollow fiber mat was heat-sealed and cut into 0.85” x 0.85” squares. Ten of these squares were layered in the same orientation

and melted on all four sides to create a single fiber pack, until its lateral dimensions were 0.615" x 0.615". Seven of the fiber packs were fitted into 1.34"-long square polycarbonate tube (ID = 0.625", Part # 3161T21, McMaster-Carr, IL) for a total fiber surface area of 400 cm^2. Custom-made polycarbonate square caps were fitted onto both ends of the tube and sealed with silicone RTV (McMaster-Carr, IL). The other end of the square cap was fitted with thread-to-barbed adapters (Qosina, NY). The completed device is shown in **Figure 3.2c**.

Rabbit Study, Circuit Preparation: The micro artificial lung was attached in a veno-venous extracorporeal circuit configuration **(Figure 3.2d).** The device inlet circuit components consisted of: 7 cm of 60-cm-pressure tubing with four side-holes serving as inflow cannula; male luer with spin lock-to-barb connector (Qosina, NY); 75 cm of 3/16" ID tubing; 3/16"–1/4" polycarbonate reducer; 9 cm of ¼" ID tubing; 3/16"–1/4" polycarbonate reducer; 5 cm of 3/16" ID tubing; 3/16"– 3/16" polycarbonate Luer connector (NovoSci, TX); 5 cm of 3/16" ID tubing. The device outlet circuit components are: 5 cm of 3/16" ID tubing; 3/16"–3/16" polycarbonate Luer connector; 25 cm of 3/16" ID tubing; and a 14-gauge angiocatheter (Becton Dickinson, NJ) as the outflow cannula. The circuit was coated tip-to-tip with PCB-(DOPA)4 for the coating group using the previously described methodology. The uncoated group had the same circuit components without the coating. On the day of the experiment, the circuit was primed with saline and 10 mg/kg of sodium methylprednisolone.

Acute Rabbit Study: New Zealand white rabbits (Average weight = 3.6 +/- 0.4 kg) were initially sedated with subcutaneous injection of 30 mg/kg of ketamine (Vedco Inc, MO) and 5 mg/kg of xylazine (Akorn Animal Health, IL). They were then intubated and attached

to the ventilator using 100% O_2 with 1-5% isoflurane for anesthesia during the experiment. An intravenous drip of Lactated Ringer's solution was also started at 10-30 mL/kg/hr.

A 16-gauge angiocatheter (Becton Dickinson, NJ) was placed in the carotid artery for both blood sampling, MAP measurements, and drug delivery. A continuous intravenous drip of phenylephrine was then started using a syringe pump (New Era Pump Systems Inc, NY) at a rate between 0.5 and 5 μg/kg/min in order to maintain normal blood pressure. All baseline blood samples and measurements were taken at this point (see *Blood Sampling*). For circuit attachment, a 16-gauge angiocatheter was first inserted into the left internal jugular vein as the reinfusion site. Heparin infusion was then started at the left jugular incision site at 1 unit/min to prevent clot formation. For drainage cannula, a pressure tubing (VLMF120, Edwards Lifesciences, CA) was cut to a length of 6 cm with a bevel in a direction opposite of cannula's curvature to prevent suctioning against vessel wall. Three side-holes were cut out near the beveled tip, and this cannula was inserted into the right internal jugular vein as the drainage cannula until its tip reached the right atrium. Blood flow through the circuit was maintained at 45 mL/min with a roller pump (COBE, CO). Heparin infusion rate was kept between 60 and 120 units/hour to maintain ACT between 220 and 300 seconds.

Rabbit Study, Blood Sampling: Rabbit arterial blood was drawn for determining the activated clotting time (ACT), arterial blood gas (ABG), platelet counts, and enzyme-linked immunosorbent assays (ELISA) for p-selectin and fibrinopeptide A. These blood samples were all taken at baseline, and 10, 30, 120, and 240 minutes after circuit attachment. Additionally, ACT was also taken at 60 and 180 minutes. Heparinized syringes were used for ELISA samples. For platelet counts, syringes were citrated at 9:1 v/v ratio blood:ACD

(Santa Cruz Biotechnology, CA). Arterial blood gas measurement was taken using heparinized syringe.

The activated clotting time was measured using a Hemochron Response Whole Blood Coagulation System (Accriva Diagnostics, San Diego, CA). Arterial blood gas (ABG) was measured with ABL Flex 800 gas analyzer (Radiometer, Copenhagen, Denmark) for monitoring health and measuring hemoglobin level; and platelet counts were taken with a Z1 Dual Threshold Coulter Counter (Beckman Coulter, Brea, CA) following the manufacturer's specifications for platelets. For the ELISAs, 2 mL of whole blood was collected in a heparinized syringe and then centrifuged at 1000g for 20 minutes. The plasma supernatant was collected and immediately frozen at -20 ^{o}C. ELISA kits (MyBioSource, San Diego, CA) were used for rabbit soluble p-selectin (Catalog #: MBS011457) and rabbit fibrinopeptide A (Catalog #: MBS013487). The instruction manuals were followed for measuring plasma level of each protein.

Rabbit Study, Digital Data: The same procedure was followed from that of chronic sheep study to measure blood pressures, flow rate, and resistance.

Rabbit Study, Device Detachment and Autopsy: Four hours after the circuit attachment, rabbits were given 10,000 units of heparin intravenously in preparation for circuit detachment. The entire circuit was then detached and flushed with saline until the effluent became clear. After circuit removal, rabbits were euthanized with 2 mEq/kg of intravenous potassium (Hospira, IL). The micro artificial lung was then removed from the rest of the circuit and dried with a gentle stream of air until no moisture could be detected. The device was weighed, and the change in device weight between the beginning and end of the experiment was recorded as the clot weight. The micro artificial lung was then fixed in 2%

glutaraldehyde solution in 0.2 M phosphate buffer for scanning electron microscopy. Hollow fiber pieces were excised from the center of the fiber layer at the inlet, middle, and outlet of the bundle. These samples were dehydrated with 25, 50, 75, and 100% ethanol solutions in water. Fiber samples were then sputter coated with platinum at 3 nm thickness. The images were taken with 5 kV accelerating voltage, spot size of 3.0, and magnification levels between 50 and 2000 (Philips XL-30, Netherlands).

Rabbit Study, Data Processing and Statistical Analysis: Prior to statistical analysis, platelet count and clotting factor levels were first corrected for hemodilution caused by circuit attachment, and normalized to baseline, pre-attachment, as follows: corrected data = raw data × $\text{Hemoglobinb}_{\text{Baseline}}/\text{Hemoglobin}_{t=10\ \text{min}}$ (Fig. S1: Hemoglobin data). A mixed linear model was used to analyze clotting factor levels, ACT, log(resistance), and platelet count in the same fashion as the sheep study. The device clot weight was compared using Student's t-test. The clotting factor levels and platelet count were represented as the change from its baseline value.

3.3 Results and Discussion

3.3.1 *Sheep Study results*

Five sets of devices were tested in two different sheep. Three sets of devices were attached to the first sheep and two sets to the second. One PCB-(DOPA)4 device from the first sheep was removed early at a 12-hour mark due to a high resistance measurement. However, this device showed low amount of clot formation that did not match up with its

recorded resistance, and it was found later that the same pressure transducer was malfunctioning. Hence, this PCB-(DOPA)4 device was removed from subsequent analysis, leaving N = 4 for PCB-(DOPA)4. The entire second set from the second sheep was also terminated early at a 34-hour mark due to early euthanasia. The average ACT across all time points for both sheep was 152 ± 30 s (mean ± SD). The log(resistance) (mmHg L^{-1} min) across all time points for each surface type is shown in **Figure 3.3a.** The PCB-(DOPA)4 coated devices had the lowest resistance and the smallest deviation between sets. The failure curve from these same sets of devices is shown in **Figure 3.3b.** PCB-(DOPA)4 had the lowest failure rate of 25%, followed by ARGET-ATRP (40%), uncoated (60%),. Whereas more sheep experiments could have been performed to achieve statistical significance, we decided to instead proceed with the rabbit experiment to conduct a study that focuses on one type of coating under a more clinically relevant setting. For this following study, PCB-(DOPA)4 coating was selected as it showed the lowest rate of failure.

3.3.2 *Rabbit Study results*

Initially, seven rabbits were used for the uncoated control group, and six rabbits for the PCB-(DOPA)4 group. However, 1 rabbit in the uncoated control group and 1 rabbit in the PCB-(DOPA)4 group were completely discarded because the ACT did not fit the proposed clinical range. Two rabbits' platelet count data, one from each group, were also discarded because both cases showed an abnormally low platelet count at baseline ($<1x10^8$ cells/mL) that increased to more than 1.5 x 10^8 cells/mL at the 10-minute mark, leaving N = 4 for PCB-(DOPA)4 and N = 5 for uncoated.

The ACTs were not significantly different between the two groups (Figure S1, p = 0.21) over the 4-hour period (uncoated = 241 ± 43 s, PCB-(DOPA)4 = 260 ± 44 s, mean ±

SD). The average baseline platelet count (x 10^8 platelets/mL, mean ± SD) for uncoated and PCB-(DOPA)4 was 1.60 ± 0.20 and 1.76 ± 0.24, respectively (N = 4 and 5, respectively).

The change in device weight was significantly different between groups ($p < 0.05$, **Figure 3.4a)**. The coating group had 59% less clot weight than the uncoated after the 4-hour study. The clot formation throughout the study was recorded by measuring device's blood flow resistance **(Figure3. 4b)**. Both groups showed a common trend, in which there was an initial spike in the first 2 hours, but the value dropped back down and stabilized for the remainder of the experiment (**Figure 3.4b).** The uncoated control's resistance was consistently higher in magnitude than PCB-(DOPA)4, but there was no significant difference between the groups due to the large variation between rabbits ($p = 0.18$). The scanning electron microscopy images showed that the PCB-(DOPA)4 coating reduced microscopic clot formation on both the hollow gas exchange fibers **(Figures 3.5a & b)** as well as the finer weaving fibers **(Figures 3.5c & d).** These results indicate that the gross clot formation was reduced with PCB-$(DOPA)_4$ tip-to-tip coating.

To better understand how PCB-(DOPA)4 reduced thrombus formation, blood coagulation and platelet activation were studied with ELISAs and platelet counts. The plasma FPA level, produced as a byproduct from fibrin generation, is shown in **Figure 3.6** as a change from the baseline. For both groups, there was an increase within 30 minutes after attachment, but this spike was suppressed in the coated case. The peak occurred after 10 minutes for uncoated and 30 minutes for the PCB-(DOPA)4, but the average FPA level was consistently higher in the uncoated case. The overall difference approached statistical significance between groups ($p = 0.06$).

3.3.3 Discussion on coating methods.

This study was conducted to evaluate the efficacy of PCB coatings in two steps. First, each grafting methodology was carried out over miniature artificial lung surfaces, and the coated lungs were tested in a parallel veno-venous circuit for a fair assessment of coatings. The anticoagulant function of the most promising method was then studied independently in a four-hour rabbit veno-venous model with a clinically relevant ACT. Although the devices used in the sheep study are smaller than those used in clinical ECMO, the 0.1 m^2 surface area and the packed bed geometry of the fiber bundle still pose a challenge for achieving a uniform surface coverage. Furthermore, the miniature artificial lung in the study consists of multiple of materials: PDMS potting, tubing, and hollow fibers; polypropylene weaving fibers; PETG housing; and polyurethane filling. Achieving an effective coating over various surface compositions and geometries using one fixed coating process is challenging.

The ARGET coating had only a slightly lower failure rate than the uncoated. The PCB-(DOPA)4 coating not only had the lowest failure rate of 25%, but also had the most consistent results within the group. DOPA is a versatile adhesive molecule that can stably attach to a variety of surfaces through different possible mechanisms.[29-36] Hence, it may be that PCB-(DOPA)4 was the most effective in part because there are multiple surface materials like artificial lungs. The ARGET-ATRP ‘graft-from” methodology can theoretically achieve a higher grafting density by covalently attaching initiator molecules to the surface and then polymerizing CB monomers. However, ARGET-ATRP is costlier and attaching initiators is challenging. In the current study, a piranha solution was used to graft the initiators, serving as a powerful oxidizing agent to hydroxylate organic surfaces. In addition to its safety risks, the reagent also raises a concern about material degradation

that may lead to premature device failure. Regardless, ARGET-ATRP devices had highly variable resistance values between sets and exhibited a similar failure trend as the uncoated in this study **(Figure 3.3b)**. This may be due to the challenges of scaling up the ARGET-ATRP methodology to larger, more complex surfaces compared to smaller, simpler surfaces tested in previous studies. [30]

Overall, the sheep study showed that the DOPA methodology may be the most effective method for attaching PCB chains to artificial lung surfaces. Moreover, the sheep model evaluated PCB-coating efficacy over a large, complex surface under rigorous whole blood environment, which has never been demonstrated before. However, this alone does not provide enough information about the effects of coating. Because of the parallel configuration of the extracorporeal circuit, the benefits of one successful coating on the coagulation system may be confounded and obscured by the presence of other less successful ones, the control device, and the uncoated circuit. The polycarbonate connectors present throughout the circuit are especially prone to thrombus formation because they introduce geometrical steps in the circuit, so their presence puts even more of a challenge for the coatings. Finally, there was no continuous administration of heparin anticoagulation to sheep. The rationale for this experimental design was to accelerate clotting and observe measurable changes within the 36-hour time frame. Otherwise, the duration would have to be extended to at least one week for clinical oxygenators to actually fail. [23-25] With the low ACT range specified in this experiment, the surfaces were subjected to an abnormally highly procoagulant bloodstream. The PCB coatings in this study can only repel non-specific adsorption but have no means of inhibiting activated platelets or coagulation factors. Thus, coatings will have limited benefit when the remainder of the circuit,

particularly the circuit inlet, are rapidly producing thrombus. In a similar study using ECMO without anticoagulation, Lai *et al*. found a precipitous increase in failure rate at around 36 hours, even in devices with relatively slower clot formation. [43].

The follow-up rabbit study was thus designed to examine the devices using a more clinically relevant ACT range. Only one type of coating was tested per animal to focus on each surface type's effect on the coagulation system. Furthermore, the entire circuit was coated tip-to-tip to minimize the confounding effects of uncoated surfaces, and the rabbit was also given a continuous drip of heparin to keep ACT at a clinically-relevant range of 220 and 300 seconds. Hence, the experimental design of the rabbit study better reflects how the coatings will be used in future clinical applications.

In the rabbit study, the macroscopic clot formation was significantly reduced with PCB-(DOPA)4 coating as demonstrated by the significant reduction of device clot weight. Furthermore, the electron microscope images also confirm that micron-scale clot formation was suppressed over both hollow and weaving fiber surfaces. Finer weaving fibers tend to generate denser clots compared to the hollow fibers and can be especially challenging to coat.[29] These 10 μm-diameter fiber strands are tightly wound together, so the interstices form stagnant regions that can easily entrap platelets and accumulate procoagulant factors, making them challenging areas for reducing fouling. The SEM images from this study suggest that the PCB-$(DOPA)_4$ coating was grafted successfully even to the fine weaving fibers and reduced coagulation over these areas as well.

The other supporting data suggest that the PCB-$(DOPA)_4$ coating reduced clot formation by reducing the contact activation of coagulation cascade. The coating's effect becomes apparent in the first 60 minutes, as seen in the FPA level and the device resistance.

The most marked increase in FPA occurs in the first 10 minutes for the uncoated case, but this was mitigated with PCB-$(DOPA)_4$ coating. The large surge in FPA level can be attributed to the initial exposure of blood to artificial material which elicits the most extreme response from the intrinsic pathway. With the low-fouling coating, the contact activation of the intrinsic pathway was reduced, so the rate of FPA generation decreased. The rapid increase in resistance also occurred within the first hour for the uncoated but substantially less in the PCB-$(DOPA)_4$ group. The contact activation led to rapid formation of thrombus within the uncoated device, occlusion of the blood flow, and consequently the marked increase in resistance. Because the peak in resistance occurred at different time points between devices, this led to large variability between devices, so the difference approached, but did not achieve, significance.

The FPA and resistance data showed a similar trajectory over the 4-hour period: a rapid increase, followed by a slight drop, and finally a plateau. The contact activation in the initial stage leads to acceleration of the coagulation process, resulting in the rapid rise in fibrin formation and thus FPA level and device resistance. After the initial spike, clot formation slows, presumably due to exhaustion of procoagulant zymogens and activation of the fibrinolytic system. While clot is forming, fibrin also catalyzes fibrinolysis by increasing the rate of conversion of inactive plasminogen to plasmin,[45-49] and enhancing clot breakdown in the micro-lung. The end-result in this early experimental phase is a shift from rapid coagulation toward clot dissolution.

Whereas the coating's clearly reduced coagulation, there was no significant effect of PCB-$(DOPA)_4$ coating on the p-selectin expression or the platelet count. This result appears to contradict previous studies that have shown that the PCB-(DOPA)4 coating

reduces platelet attachment to PDMS surfaces by 77% in an 8-hour flow circuit experiment.[17] In the current experiment, however, we measured systemic platelet counts and function, rather than surface platelet adhesion. Due to its ability to stop overall clot formation, the coating may keep platelets from sticking to the surface and forming clot, but its effect on circulating platelets appears to be small during ECMO and most likely confounded by pump-induced platelet activation. Roller pumps cause shear-induced activation and micro-aggregation of platelets.[42-44] It is, therefore, likely that the pump was the dominant cause of systemic platelet activation and consumption in this experiment, despite coating-induced anticoagulation in the fiber bundle. This also suggests that any coating's effect will be blunted by pump-induced platelet activation.

Overall, these results suggest that PCB can reduce coagulation during long-term, *in vivo* study of full-scale artificial lungs. It is common for coatings to work well with single protein solutions or even plasma, but to be inadequate when tested *in vivo* against whole blood.[46-68]. Previous study showed that glucose sensors coated with lightly crosslinked PCB hydrogels maintained high sensitivity and linearity over 42 days in whole blood.[49] However, this presented study featured a far larger, far denser surface area with far greater geometric complexity. Success in this study suggests that further studies examining PCB-$(DOPA)_4$ coatings during long-term, weeks-long ECMO at clinically relevant ACTs should be pursued. With continuous anticoagulant administration, tip-to-tip surface coating, and optimized device design for blood flow through the device, a better coating performance would be expected to achieve a longer device lifetime. However, larger devices also possess larger fiber bundles and care will need to be taken to ensure uniform coatings throughout. If successful in that setting, PCB coatings should be able to reduce thrombotic

complications and perhaps bleeding complications, if heparin concentrations can be reduced. Ultimately, this could reduce patient mortality as well.

3.4 Conclusions

Artificial lung prototype devices coated with e PCB-DOPA conjugates as well as their uncoated control devices were attached in parallel within a veno-venous sheep extracorporeal circuit with no continuous anticoagulation (N = 5 circuits). The results indicated that the PCB-(DOPA)4 approach showed the least increase in blood flow resistance and the lowest incidence of device failure over 36-hours. Another 4-hour rabbit study with veno-venous micro-artificial lung circuit at a higher activated clotting time of 220–300 s (N = 5) proved that PCB-$(DOPA)_4$ reduced fibrin formation ($p = 0.06$) and gross thrombus formation by 59% ($p < 0.05$).

3.5 Figures

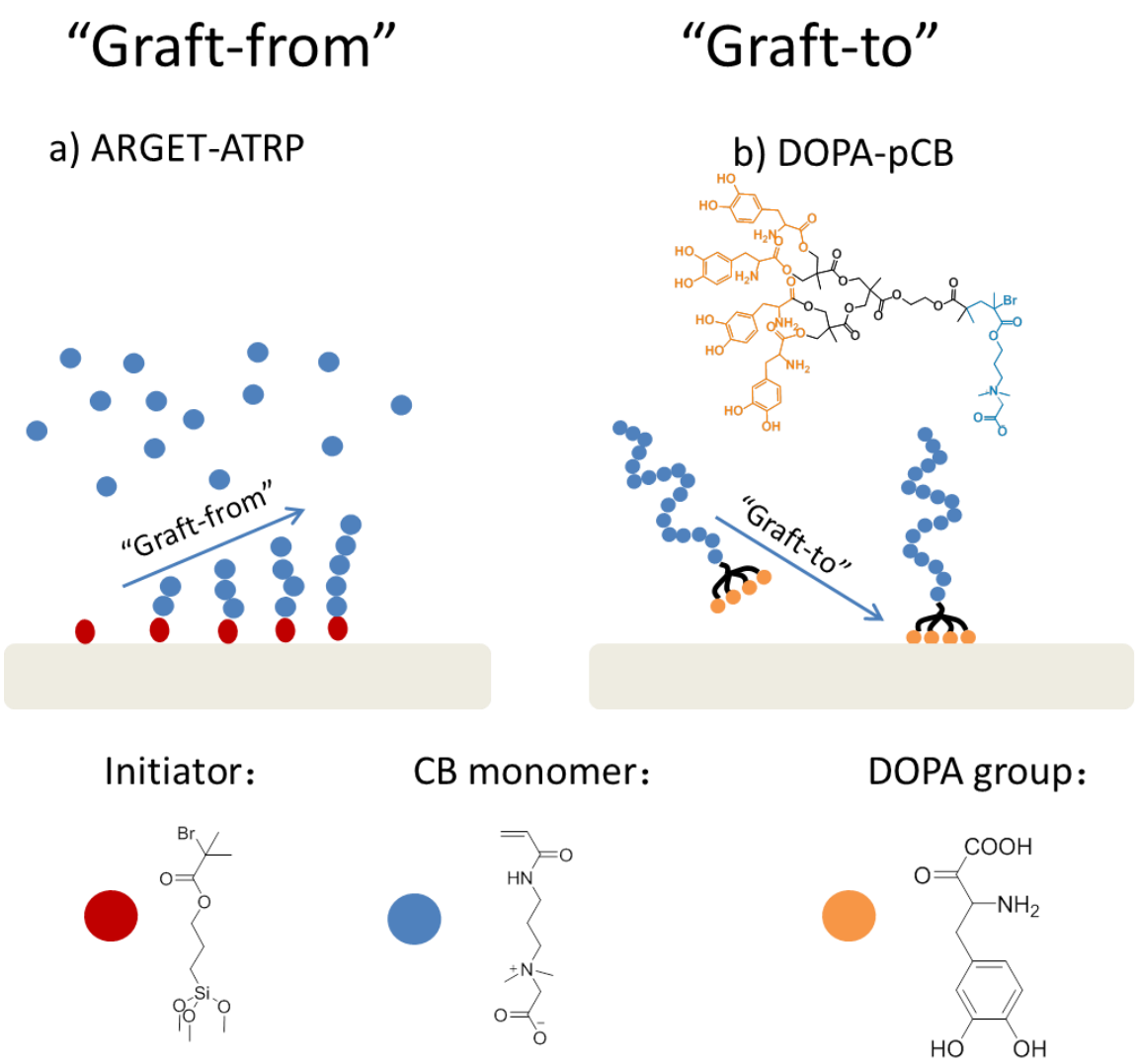

Figure 3.1 Schematics illustrating different grafting techniques for PCB, a) ARGET-ATRP, b) PCB-DOPA

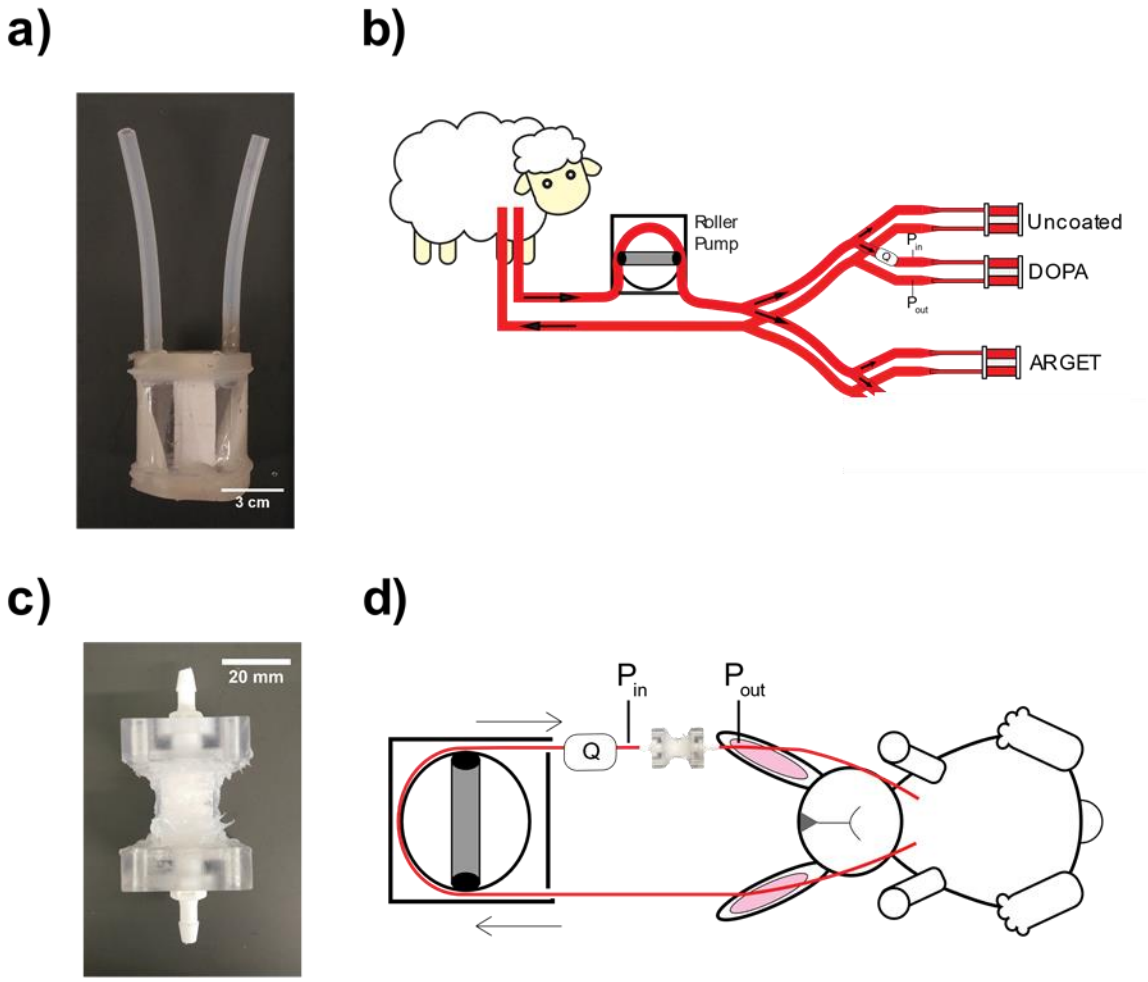

Figure 3.2 **Fabricated artificial lungs and animal extracorporeal circuit diagrams: a) miniature artificial lung (fiber surface area = 0.1 m^2); b) sheep veno-venous parallel extracorporeal circuit featuring miniature artificial lungs coated with one of *three* methods (uncoated control, "graft-to" PCB-(DOPA)4, "graft-from" ARGET-ATRP). Each device's thromboresistance is tracked by measuring flow rate (Q) with flow probe and pressure drop ($P_{in} - P_{out}$) with pressure transducers to calculate resistance; c) micro artificial lung used for rabbit study (fiber surface area = 400 cm^2); d) rabbit veno-venous extracorporeal circuit, with or without tip-to-tip PCB coating**

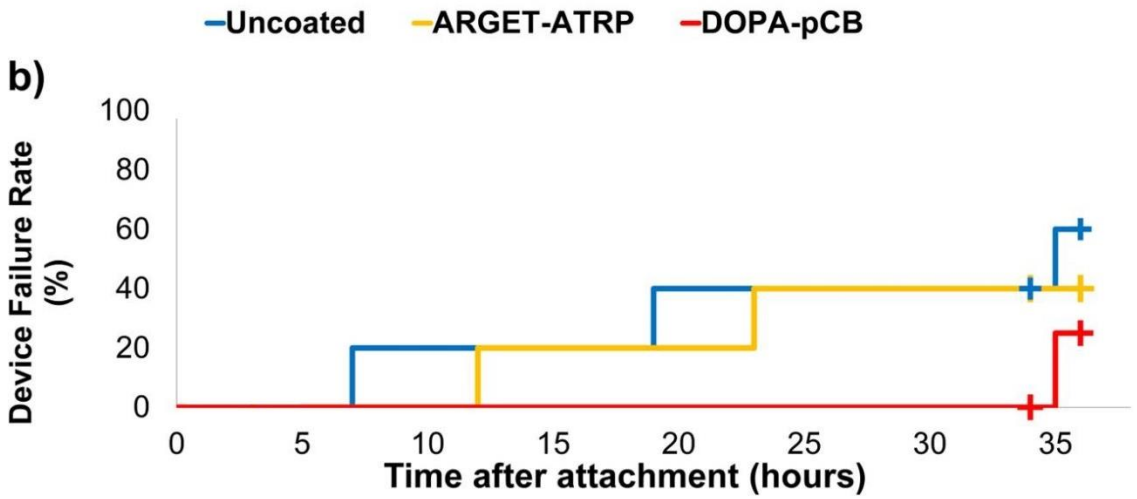

Figure 3.3 Device failure curve plotted over the 36-hour period for the same set of devices; plus signs indicate censored events.

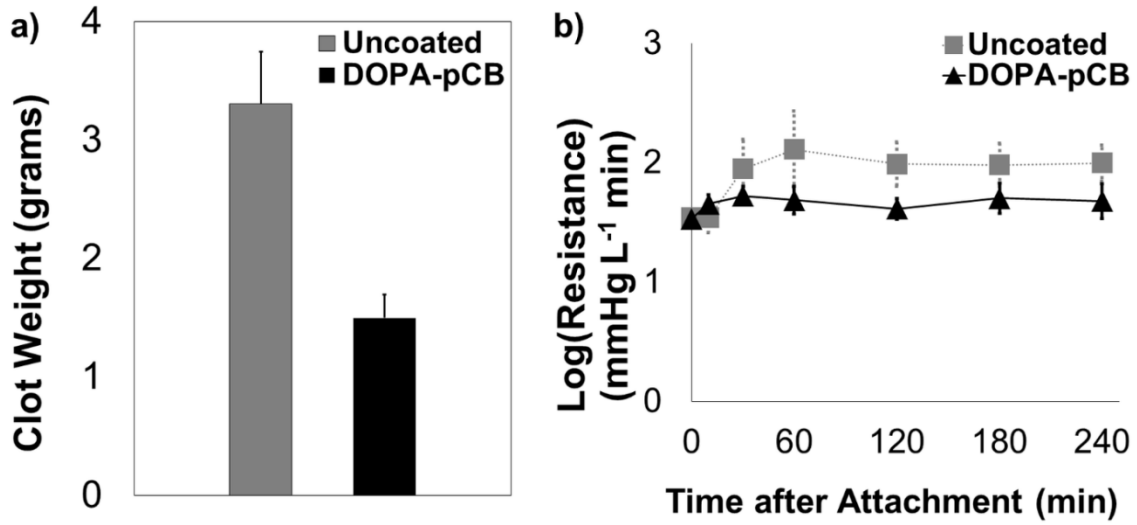

Figure 3.4 Quantitative measurements of thrombus formation: a) total clot formation inside the micro artificial lung at end of the 4-hour rabbit study, $p < 0.05$, $N \geq 4$; b) log(Resistance) for micro-artificial lung in the 4-hour rabbit study, $N \geq 5$, $p = 0.18$. Error bars = S.E.M. for both figures

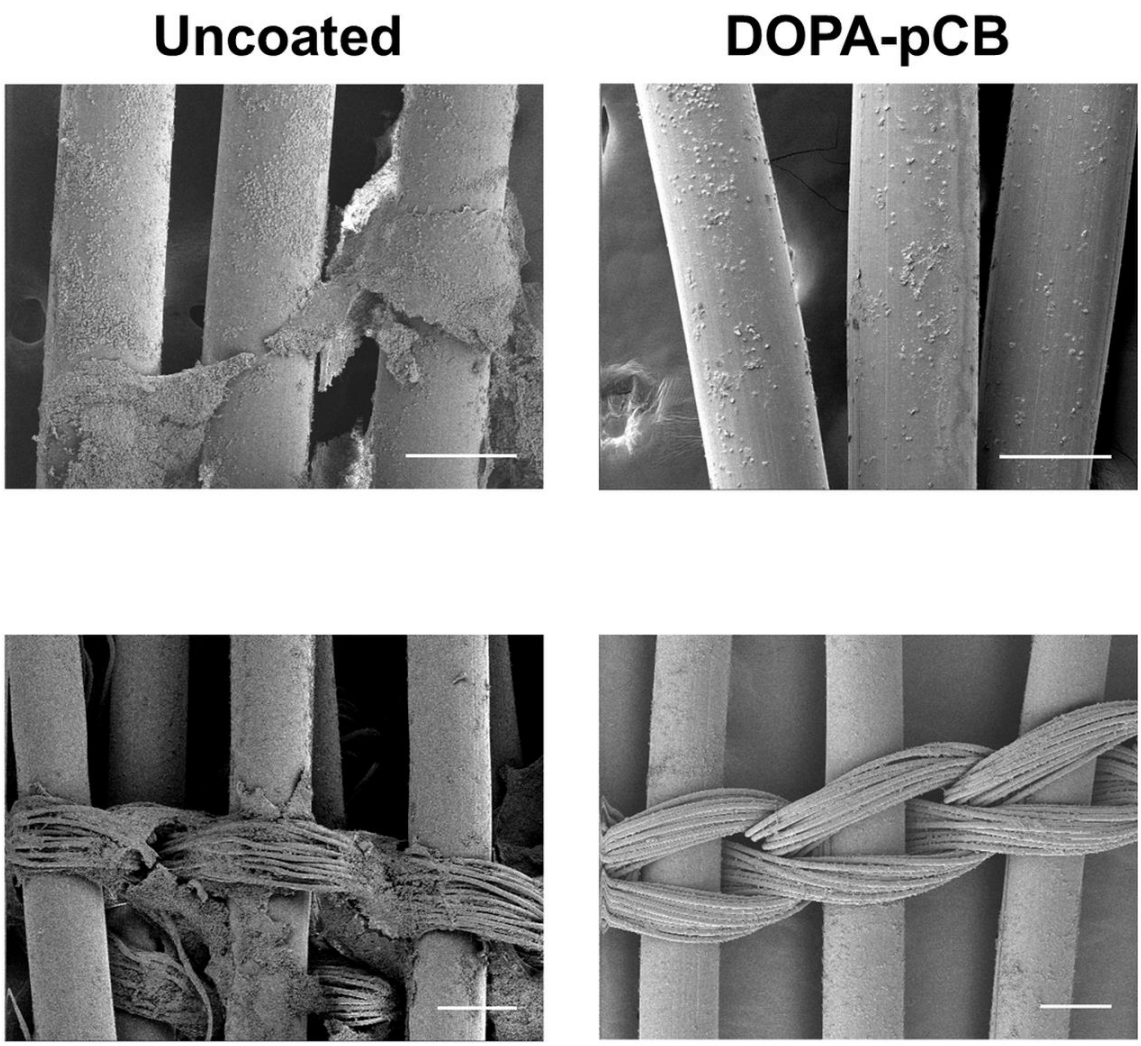

Figure 3.5 Scanning electron microscope images of uncoated (left column) and PCB-(DOPA)4 (right column). Hollow fibers (top row) and finer weaving fibers (bottom row) are both shown. Scale bar = 200 μm for all four panels

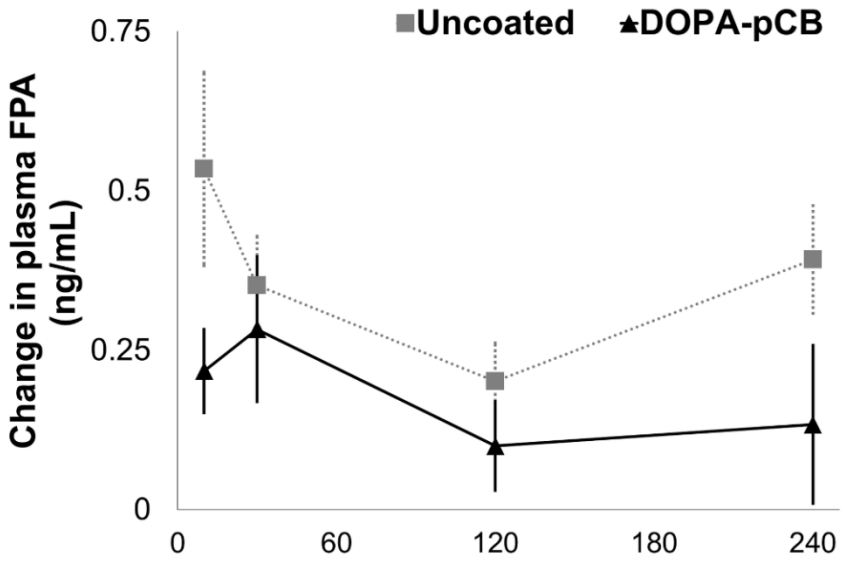

Figure 3.6: The change in plasma fibrinopeptide A(FPA) level from baseline measurements, p = 0.06, N ≥ 5, error bar = S.E.M..

Chapter 4 Paper Sensor prepared by dip-coating with a Zwitterionic Poly(carboxybetaine) Polymer Conjugate containing multiple DOPA Groups for Biosensing in Complex Media

Cellulose paper is an ideal diagnostic platform for low-cost, easily disposable and lightweight implementation, but requires surface modification to achieve detection with high sensitivity and specificity in complex media. In this work, a polymer-catechol conjugate containing a super-hydrophilic nonfouling poly(carboxylbetaine) (PCB) and four surface-binding L-3,4-dihydroxyphenylalanine (DOPA) groups, PCB-$(DOPA)_4$, were applied onto a paper-based sensor surface via a simple "graft-to" immersion process to render the surface with both nonfouling and protein functionalizable properties. This dip-coating technique is effective, convenient and robust as compared to the "graft-from" techniques reported previously with similar nonfouling properties. The coated paper sensor showed both increased analyte diffusion rate and improved sensitivity of glucose detection in human blood serum. The capability of PCB-(DOPA)4 modified paper sensor for specific antigen-antibody detection was demonstrated via the covalent immobilization of bovine serum albumin antibody (anti-BSA) and fibrinogen antibody (anti-Fg) onto the PCB-coated surface via simple 1-ethyl-3-(3-dimethylaminopropyl)-carbodiimide and N-hydroxysuccinimide (EDC/NHS) chemistry.

4.1 Introduction

The development of new point-of-care diagnostic devices is vital for health in both industrialized and developing countries. However, the realization of this concept relies on the development of simple sensing platforms for the highly sensitive detection of target

biomarkers in complex media such as undiluted human blood plasma and serum or urines.1,2 Although conventional instrumentation is able to provide quantitative measurements, its widespread use is limited because of its large instrument size, high cost, large sample volume and required trained personnel.2 Paper has several advantages as it is thin, lightweight, available in a large range of thicknesses with different properties, and easily stacked, stored, and transported. Most importantly, paper is the least expensive platform for assay development and often enables faster detection. Other significant benefits include being chemically modifiable, exhibiting a "white" background for sensing, and being easily disposable. Also, it is compatible with printing technologies, which can be used to fabricate patterns for running multiple diagnostic assays on a single strip of paper using a small volume of sample. Paper sensors have a plethora of applications such as metabolite monitoring, food and water safety inspection, and national security guarantee against numerous diseases.

Despite these benefits, state-of-the-art paper-based diagnostic methods suffer several disadvantages, especially when they are applied to detection in complex media. First, most assays rely on cellulose papers where detection agents are physically adsorbed and dried.[50-53] This leads to the drifting and denaturing of the detection ligands (e.g., antibodies). Second, cellulose paper has limited hydrophilicity. This reduces sample retention on paper surfaces. Sample that reaches the final detection zone is typically less than 50% of the original due to evaporation.[54] Third, unmodified cellulose paper is insufficient to resist nonspecific adsorption in complex media. Detection sensitivity is significantly reduced because of the loss of un-immobilized detection agent, the loss of target analyte during

transport to the detection zone,5 and background noise from nonspecifically adsorbed protein.[54,55]

To address many of these shortcomings, we demonstrated surface modification on a cellulose paper sensor with zwitterionic poly(carboxybetaine) (PCB) for detection in complex media.[57] PCB is an attractive material for paper sensors for the following reasons: (a) PCB is highly resistant to nonspecific protein adsorption (<0.3 ng/cm2) from 100% blood plasma and serum;[56-58] (b) PCB has abundant functional groups (COOH) for the effective and convenient immobilization of bio-recognition elements (e.g., antibodies) via simple 1-ethyl-3-(3-dimethylaminopropyl)-carbodiimide and N-hydroxysuccinimide (EDC/NHS) chemistry. [59-60] In previous work, PCB brushes were coated onto a cellulose paper using surface-initiated atom transfer radical polymerization (SI-ATRP), where an initiator was covalently immobilized on the paper surface first, followed by grafting polymer brushes from the paper. [57] The PCB modified paper sensor enabled faster detection of glucose and other specific antigens with higher sensitivity on undiluted human serum than bare cellulose. Although the "graft-from" approach using ATRP may render high surface packing density and excellent non-fouling performance, this coating method usually requires relatively skilled polymer synthesis and oxygen-free conditions.[58-64] Moreover, it is difficult to apply the SI-ATRP method to sensor surfaces with large surface area or complex geometry. The "graft-to" dip-coating method is highly desirable for practical applications, but it is relatively difficult to achieve high surface packing densities, particularly rendering ultralow fouling surface properties.[65-67]

The zwitterionic polymer is highly water-soluble and the competition between peel-off strength from surrounding water molecules and surface adhesion strength dramatically

influences coating density and stability. It is essential to have a strong surface-binding group on the zwitterionic polymer. Catechol-containing molecules are excellent candidates for this purpose. Waite and Israelachvili et al. [68] reported that the catechol group found in mussel foot proteins is highly responsible for surface adhesion underwater. Various catechol-like molecules are shown to form stable surface-independent coatings.20-22 Among these catechol derivative molecules, L-3,4-dihydroxyphenylalanine (DOPA) is unique because it contains amine and carboxylic acid group for further polymer conjugation and has potential to form poly-DOPA.

In this work, we synthesized the zwitterionic PCB polymer with surface-adhesive DOPA groups. To increase coating binding affinity with the cellulose paper surface and maximize the device lifespan, we introduce a dendritic binding block containing four adhesive DOPA groups to create multiple pairs of interactions. This PCB-(DOPA)4 could be coated on the cellulose paper by simple immersion (Scheme 1). The dip-coated paper sensor demonstrated super-hydrophilicity, increased analyte diffusion rate and excellent fouling resistance as good as the "graft-from" method. In addition, unlike poly-dopamine commonly used for surface pre-treatment, this PCB-(DOPA)4 based "graft-to" technique gives colorless and transparent nonfouling coating in one step, which does not interfere with colorimetric detection. The PCB-(DOPA)4 modified paper sensor achieved sensitive glucose detection within a physiologically relevant range in undiluted human serum. The PCB-(DOPA)4 coated cellulose paper also demonstrated robust covalent antibody immobilization and specific antigen detection.

4.2 Experimental Section

4.2.1 Materials

Carboxybetaine acrylamide (CBAA) monomer was synthesized according to a previously reported protocol.[23] The following chemicals and materials were purchased from Sigma-Aldrich (St. Louis, MO, USA), and were used as received: Monoclonal anti-bovine serum albumin antibody produced in mouse (Anti-BSA), Anti-fibrinogen antibody produced in goat (Anti-Fibrinogen), Triethylamine (TEA, 99%), potassium iodide (KI), Glucose oxidase/peroxidase reagent, N-hydroxysuccinimide (NHS), N-ethyl-N′-(3-diethylaminopropyl) carbodiimide hydrochloride (EDC), bovine serum albumin, Alexa Fluor 568 tagged bovine serum albumin, and Alexa Fluor 488, Copper (I) bromide (CuBr, 98%), 1,1,4,7,10,10-Hexamethyltriethylenetetramine (HMTETA, 97%), tetrabutylammonium fluoride hydrate (TBAF, 98%), trifluoroacetic acid (TFA, 99%), methanol (99.9%), bovine plasma fibrinogen, phosphate-buffered saline (PBS, 0.01 M phosphate) package, and Whatman 1 filter paper. Pooled human blood serum was purchased from BioChemed Services (Winchester, VA, USA). Ethanol (200 proof) was purchased from Decon Labs. Polydimethylsiloxane (PDMS; Sylgard 184) was purchased from Dow Corning. The water used in these experiments was obtained from a Millipore water purification system with a minimum resistivity of 18.0 MΩ cm. Bovine serum albumin (96%), o-Phenylenediamine (OPD, 98%). Paper-based microfluidic devices were fabricated following our previous work8: (a) coat glass substrate with PDMS and pattern sensing channels into PDMS using laser-cutting; (b) laser-cut cellulose paper with the same pattern; (c) place patterned paper (coated or uncoated with PCB-(DOPA)4) onto the patterned PDMS substrate to form detection assay. The hydrophobic PDMS pattern formed

a hydrophobic barrier that aqueous solutions could not cross. The hydrophilic cellulose paper modified with PCB-(DOPA)4 enable aqueous fluids to wick along the channel.

4.2.2 Synthesis of N,N-Dimethyl-cysteamine-carboxybetaine

Polymerization of PCB polymer-DOPA conjugates: The DOPA containing initiator was synthesized as reported previously. Initiator (51.5 mg, 0.02 mmol), CBAA2 (1400 mg, 6.14 mmol), CuBr (5.74 mg, 0.04 mmol) and Methanol (10 mL) were added to a 100 mL Schlenk flask equipped with a stirring bar. The mixture was degassed by three freeze-pump-thaw cycles before the addition of HMTETA (13.87 mg, 0.08 mmol). The reaction mixture was stirred at room temperature for 24 hours. After the reaction reached a desired conversion, the solution was directly transferred onto a 3.5k dialysis bag and dialyzed against DI water for 48 hours to remove unreacted monomer and copper complex. The product was obtained as a white solid (PCB-(DOPA)4-BOC-TBDMS) after freeze-drying for 24 hours. The chemical structure was confirmed by 1H NMR (CD3OD, 500 MHz, ppm): δ 6.75-6.31 (m, 12H), 4.19-3.99 (m, 16H), 3.62-3.31 (m, 148H), .3.31-3.05 (m, 250H), 3.05-2.85(m, 486H), 2.52-2.35 (m, 158H), 1.25 (m, 36H, protons on tert-butoxycarbonyl groups), 2.21-0.82 (m,462H), 0.86 (s, 72H, protons on TBDMS groups), 0.18 (d, 48H, protons on TBDMS groups). Mn,NMR = 27000 kg/mol. SEC: Mn,SEC = 29600 kg/mol, PDI = 1.08. **(Figure 4.1a).**

Tert-butyldimethylsilyl (TBDMS) removal of PCB-(DOPA)4: To a 50 mL round bottom flask equipped with a stirring bar was added PCB-(DOPA)4-BOC-TBDMS (550 mg, 0.02 mmol), TBAF (261.4mg, 1 mmol), DCM (5 mL). The suspension mixture was stirred at room temperature for 12 hours. The mixture was centrifuged at 4200 rpm for 2 minutes to

collect precipitate and washed with DCM for three times. The product was obtained as insoluble white solid (PCB-(DOPA)4-BOC).

BOC removal of PCB-(DOPA)4: To a 50 mL round bottom flask equipped with a stirring bar was added PCB-(DOPA)4-BOC (530 mg, 0.02 mmol), TFA (228.4 mg, 2mmol), and DCM (5 mL). The suspension mixture was stirred at room temperature for 12 hours. The mixture was centrifuged at 4200 rpm for 2 minutes to collect precipitate and washed with DCM for 3 times. The product was obtained as insoluble white solid PCB-(DOPA)4. 1H NMR (CD3OD, 500 MHz, ppm): δ 6.75-6.31 (m, 12H), 4.19-3.99 (m, 16H), 3.62-3.31 (m, 152H), .3.31-3.05 (m, 262H), 3.05-2.85 (m, 494H), 2.52-2.35 (m, 158H), 2.21-0.82 (m,382H).

4.2.3 Surface coating of PCB-(DOPA)4 on a cellulose paper.

6 mg deprotected polymer was dissolved in 3 mL Tris buffer (pH=8.5) in a 5 mL centrifuge tube. A clean cellulose paper (0.5cm x 0.5cm) was placed into the tube and submerged for 24 h. The cellulose paper coated with PCB-(DOPA)4 by this method was washed with DI water twice and dried with airflow before the test.

4.2.4 Protein adsorption measurements.

Protein adsorption examined by microscopy: After being equilibrated with PBS overnight, the PCB-(DOPA)4 modified and unmodified cellulose papers were placed into individual wells of a 24-well tissue culture plate and immersed in 1 mL of 1 mg/mL FITC-

conjugated bovine serum albumin at room temperature for 30 min and then rinsed with PBS three times. Protein adsorption was then observed under a confocal microscope.

Protein adsorption evaluated by enzyme-linked immunosorbent assay (ELISA): PCB-(DOPA)4 modified and unmodified cellulose papers were put into a 24-well plate followed by adding 0.5 mL of 1 mg/mL fibrinogen from human plasma at 37 °C for 90 min. The substrates were then rinsed five times with 0.5 mL of PBS and incubated in BSA, (1 mg/mL in PBS pH 7.4) solution for 90 min at 37 °C. The substrates were rinsed with PBS five times, transferred to new wells, and incubated in a 0.5 mL PBS (pH 7.4) solution containing 5.5 μg/mL of horseradish peroxidase (HRP) conjugated anti-fibrinogen for 30 min at 37 °C. The substrates were rinsed 5 times with 0.5 mL of PBS and transferred into clean wells, followed by the addition of 0.5 mL of 0.1 M citrate-phosphate buffer (pH 5.0) containing 1 mg/mL OPD and 0.03% (v/v) hydrogen peroxide. After incubation for 20 min at 37 °C, the enzyme-induced color reaction was stopped by adding 500 μL of 1 M H2SO4 to the solution in each well, and finally the absorbance of light intensity at 492 nm was determined by a micro-plate reader. The absorbance from unmodified cellulose paper was equivalent to 100% for calculating relative fouling values.

4.2.5 Glucose assay and antibody functionalization assay.

The glucose assay is based on the enzymatic oxidation of iodide to iodine, in which a color change from clear to brown occurs in the presence of glucose. In an assay, 0.6 M solution of potassium iodide (1.0 μL) followed by a 1:5 horseradish peroxidase/glucose oxidase solution (1.0 μL; 15 units of protein per mL of solution) was spotted onto the cellulose paper substrate. The spotted reagents were allowed to dry at 25 °C for 6 min.

Samples containing glucose (in PBS or undiluted human serum, clinically relevant ranges: 1 ~ 8 mM) were analyzed by dropping the solution (14 uL) onto the bottom of each test paper.

For antibody functionalization, the carboxylate groups of PCB were activated by the addition of a freshly prepared solution of 0.1 M NHS and 0.4 M EDC in water for 10 min at 25 °C. A solution of antibodies (anti-BSA or anti-Fg) concentration of 50 µg/mL in 10 mM HEPES buffer pH 7.5 was prepared. The solution was spotted onto the activated substrate and allowed to react for 30 minutes. The functionalized surface was then washed for a short time with 10 mM sodium carbonate buffer solution containing 0.3 M NaCl at pH 10 to remove non-covalently bound ligands. Along with protein immobilization, the remaining activated groups were also deactivated. After antibody immobilization, a mixture of fluorescently tagged BSA (red, 50 µg/mL) and fibrinogen (green, 50 µg/mL) proteins in PBS was wicked through the channel followed by washing with PBS buffer (5 times).

4.2.6 Detection and analysis method.

All digital images were taken with a Canon T3i digital camera with high resolution (18.0 megapixels) and processed with ImageJ software. The camera was operated under identical conditions: lighting was provided by a fluorescent lamp; the lens aperture was set at F/8.0; the exposure time was set at 1/5 s. The camera was placed 22 cm from the paper sensors on a static tripod support. Images were captured in ~ 5 min intervals following the addition of the glucose solution. ImageJ was used to analyze the color changes of the test zone quantitatively. To do this, a 10 × 10 pixel square area was chosen with the cursor. The “mean gray value” option was selected from the mean intensity toolbar. The value was

between 0 (black) and 255 (white). Smaller values indicated darker colors. For each sample, three readings were obtained from both the reference and test zones by varying the location of the area being measured. The average values were obtained from these readings and the intensity was calculated thereafter. To reflect the real situation, relative intensity was obtained by comparing the mean gray value of the test zone (top side of the paper sensor, circular area) and that of the reference zone (right side of the paper sensor, rectangular area). Thus, the relative intensity is a function of the contrast between the varying darkness of the test zone and the white reference area. Higher relative intensity was therefore attributed to test results with darker color.

4.3 Results and Discussion

4.3.1 Synthesis and characterization.

To anchor a zwitterionic polymer to a surface strongly, more catechol groups conjugated to the end of the zwitterionic polymer chain would help. Zwitterionic poly(sulfobetaine)-catechol conjugates were previously reported to be coated on various surfaces effectively. [72] However, PCB-catechol conjugates are harder to achieve high-surface packing densities for certain surfaces, particularly hydrophobic surfaces due to the high water solubility of PCB. [73] As shown previously, doubling binding sites can increase surface binding strength by order of magnitude. [74] More catechol groups should be able to keep highly soluble PCB polymers firmly on surfaces. In this work, we introduced four catechol groups to a PCB polymer. Crosslinking is another strategy to stabilize surface coatings. To achieve crosslinking among catechol groups, a free amine group is incorporated near each catechol group. Under aqueous conditions at pH 8.5, Michael

addition between the amine and adjacent hydroquinone will form intermolecular covalent crosslinking to increase binding strength. The catechol groups were initially protected by TBDMS while the amine groups were protected with BOC to prevent side reaction during synthesis (Scheme 2).

The DOPA-containing initiator was first synthesized. The polymerization of CB with the initiator was carried out in methanol at room temperature for 24 hours. GPC data showed that the number average molecular weight (Mn) of the polymer was 2.96×104 and its polydispersity was 1.08. TBDMS groups in the polymer were removed by reaction with 20 equimolar TBAF in DCM solution while BOC groups were removed by reaction with 100 equimolar TFA before the polymer was used for coating. 1H NMR data indicated that the number average molecular weight (Mn) of the polymer was 2.70×104, which is consistent with GPC results (2.96×104). **(Figure 4.1c)** The complete deprotection of TBDMS and BOC was confirmed by 1H NMR **(Figure 4.1b)**, where peaks from BOC and TBDMS groups disappeared after deprotection.

4.3.2 Super-hydrophilicity and nonfouling properties.

Zwitterionic PCB materials are super-hydrophilic due to strong, electrostatically induced hydration. This strong hydration increases the hydrophilicity of the cellulose paper sensor after PCB modification, resulting in faster wicking of detection solutions, thus reducing sample evaporation and detection time. To compare the hydrophilicity and wicking time of PCB-(DOPA)4 modified and bare cellulose papers, we used the same

paper-based analytical device previously reported by us.8 As shown in **Figure 4.2a**, it contained a hydrophobic PDMS mold with a particular paper sensor pattern hollow to form the sensor channel. Laser-cut paper sensors were placed inside the channels. We loaded the same amount of Waterman red (5 μL) ink onto the bottom of each test paper strip and the ink movement was monitored as a function of time. The red ink filled the whole PCB-(DOPA)4 modified paper sensor within 30s, but not the unmodified one, indicating faster detection with PCB-(DOPA)4 and better water retention ability.

In addition, super-hydrophilicity is generally considered as the key to resisting nonspecific protein adsorption. The main objective of this work is to reduce nonspecific protein adsorption on the cellulose paper sensor by surface modification with PCB-(DOPA)4. We used ELISA to measure protein (fibrinogen) adsorption for coated and uncoated cellulose papers. Protein adsorption on the bare cellulose paper was set as a reference. We compared PCB-(DOPA)4 modified cellulose papers with different dip-coating time points. As shown in **Figure 4.2b**, the PCB-(DOPA)4 modified cellulose paper for 24 h immersion time demonstrated only about 4.8% of protein adsorption. The 2 h and 4 h ones showed 8.2 % and 5.7%, respectively. We also included results from the previously reported "graft-from" method (SI-ATRP) with PCB, which is about 5.3%. Besides ELISA, we also studied protein adsorption by using FITC-BSA. The PCB-$(DOPA)_4$ modified cellulose paper dramatically reduces nonspecific protein adsorption compared with the *bare paper.*

4.3.3 Quantitative glucose detection in undiluted blood serum.

The excellent nonfouling performance of PCB-$(DOPA)_4$ on a cellulose paper supported the use of PCB-$(DOPA)_4$ modified paper sensor for bio-sensing in complex

media. In this work, we compared glucose detection in undiluted human serum by the PCB-$(DOPA)_4$ modified paper sensor and the bare paper sensor. In each detection assay, as we reported before, a 0.6 M solution of potassium iodide was spotted onto the top detection zone, followed by dipping a 1:5 horseradish peroxidase/glucose oxidase solution. After detection reagents were fully dried in air, the test solution containing 8 mM glucose was added to the bottom of each test strip. **Figure 4.3a** shows the color changes of both sensors monitored as a function of time. Here, not only did the colorimetric response occur more rapidly for the PCB-(DOPA)4 modified sensor, but also the signal intensity was significantly higher and more uniform.

We also compared the sensitivity of PCB-(DOPA)4 modified and bare paper sensors for the detection of multiple concentrations of glucose (1 – 8 mM). As shown in **Figure 4.3b,** we quantitatively analyzed detection results using ImageJ, enabling the calculation of the mean relative intensity, which was plotted as a function of time. The PCB-$(DOPA)_4$ paper sensor demonstrated higher intensity at each concentration than the bare paper sensor. These results confirm that PCB-$(DOPA)_4$ coated paper sensors can achieve a faster response, particularly in complex media. This is attributed to the super-hydrophilic properties of zwitterionic materials, which increase the rate of transport through the detection channel. Furthermore, the larger signal intensity (i.e., darker color) for the PCB-(DOPA)4 modified sensor resulted from the ultra-low fouling of zwitterionic materials, enabling more analyte to be present in the detection zone.

4.3.4 Stability and functionalization studies. Stability is also one of the important criteria to evaluate the quality of a coating. We studied the stability of dip-coated paper sensors with PCB-(DOPA)4 by storing coated cellulose papers in ambient air at room temperature

for 5, 10, and 20 days, then testing their nonfouling performance by ELISA. **Figure 4.4a** shows the results of protein adsorption measured after different storage times. After 20 days, protein adsorption is still below 8%, indicating the robustness of PCB-$(DOPA)_4$ coating.

To further examine the capability and versatility of the PCB-(DOPA)4 modified paper sensor for conjugating bioactive molecules, anti-fibrinogen (the circular region on the left) and anti-BSA (the rectangular region on the right) were covalently immobilized via EDC/NHS coupling chemistry. Antigen detection was then conducted via fluorometric binding assays, as shown in **Figure 4.4b.** A mixture of fluorescently tagged fibrinogen (green, 40 μg/mL) and BSA (red, 40 μg/mL) in PBS was flowed through the paper sensor channel, followed by washing with PBS. The circular region on the left revealed only green fluorescence while the rectangular region on the right revealed only red fluorescence, each corresponding to the expected antigen. These results demonstrate that the PCB-$(DOPA)_4$ dip-coated paper sensor is able to specifically detect analytes while resisting nonspecific adsorption using covalently coupled ligands. Specifically, the lack of any observed signal drift during detection confirms the strong covalent attachment of antibodies. Thus, PCB-$(DOPA)_4$ enables one to eliminate signal drift and signal distortion, both frequently observed using typical physical adsorption for ligand attachment, thereby further improving the performance of paper in complex media.

4.4 Conclusions

To summarize, we applied a zwitterionic PCB polymer conjugated with four DOPA adhesive groups via dip-coating to cellulose paper sensors, rendering nonfouling properties

and improving detection in complex media. Results demonstrate that this dip-coating process is much simpler and more convenient than the previously reported “graft-from” SI-ATRP method and achieves similar hydrophilicity and nonfouling performance. The PCB-$(DOPA)_4$ coated paper sensor showed accelerated diffusion of analyte and improved sensitivity of glucose detection, particularly in real-world complex media such as human blood serum. We further demonstrated the capability of PCB-$(DOPA)_4$ modified paper sensors for the specific detection of antigens after covalently immobilizing antibodies on PCB surfaces. In addition, these coatings are showed to be stable for more than 20 days.

4.5 Figures

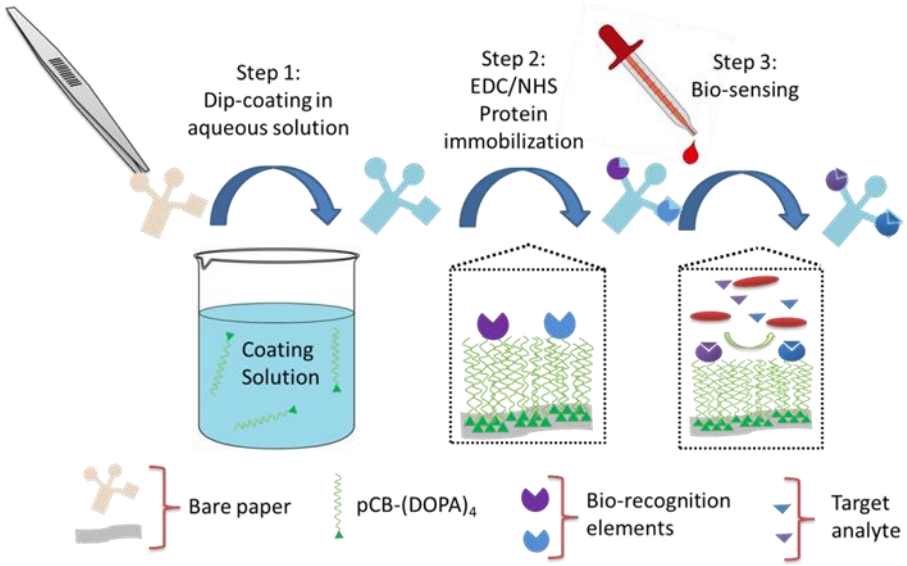

Scheme 4.1. Dip-coating a cellulose paper sensor with PCB-$(DOPA)_4$.

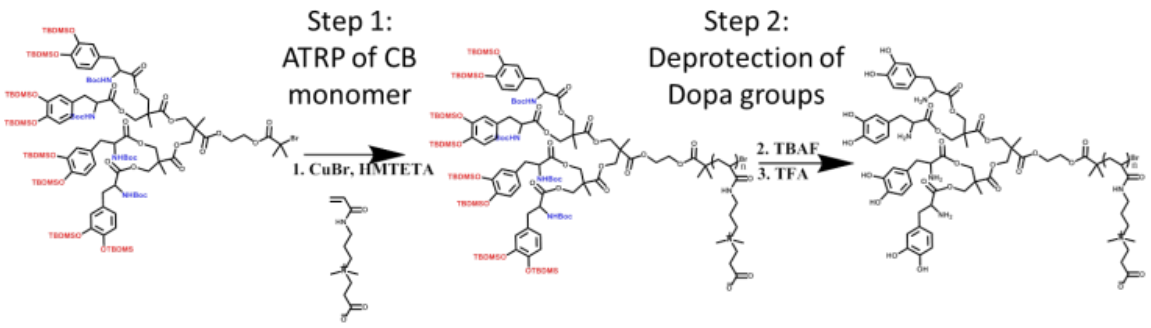

Scheme 4.2. Synthesis route of PCB-(DOPA)$_4$

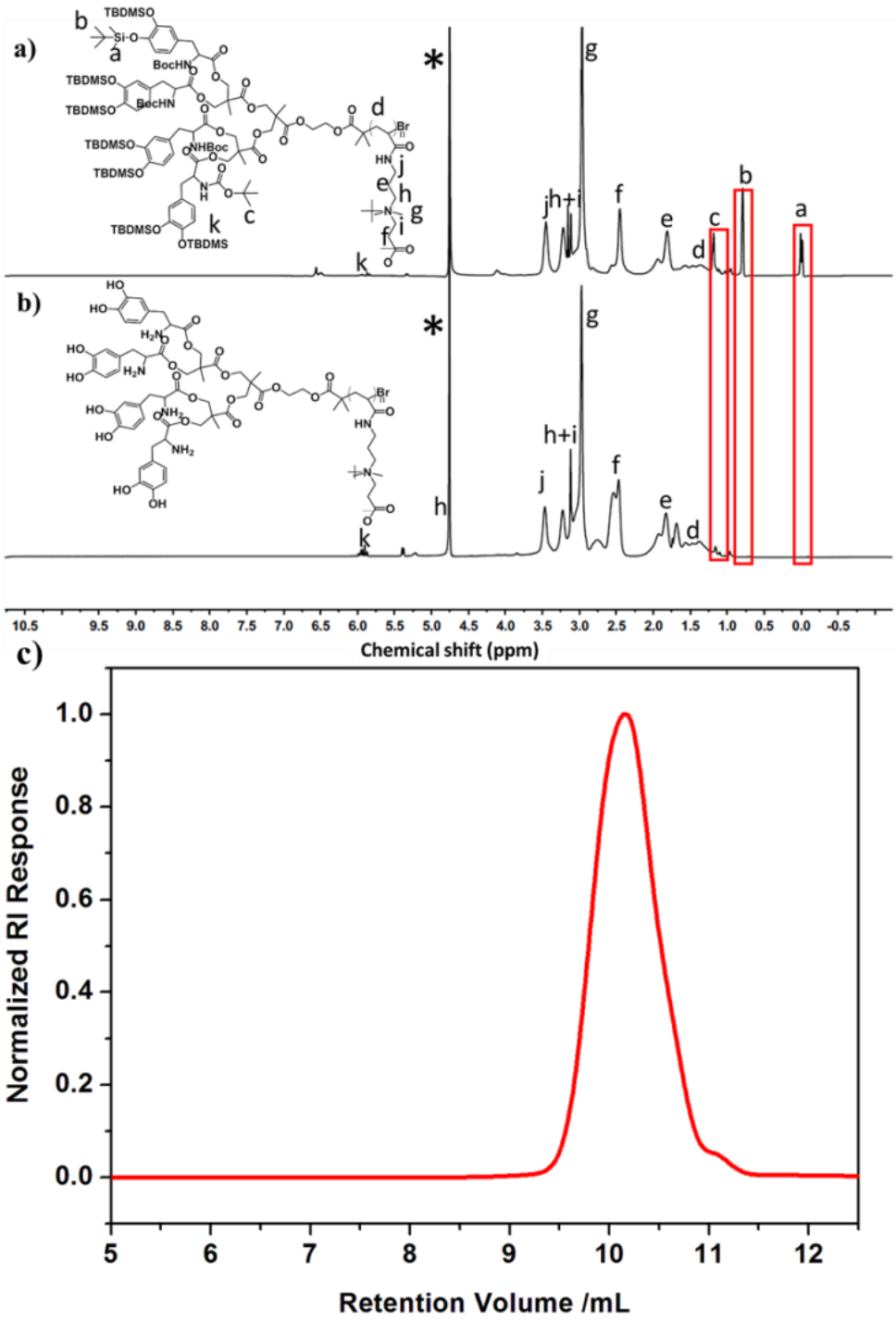

Figure 4.1. a. 1H NMR spectra, PCB-(DOPA)$_4$-BOC-TBDMS with protected BOC and TBDMS groups. b. 1H NMR spectra, PCB-(DOPA)$_4$ after deprotection of BOC and TBDMS groups. c. SEC data of PCB-(DOPA)$_4$ polymer conjugate with protected BOC and TBDMS groups. * indicates solvent peaks.

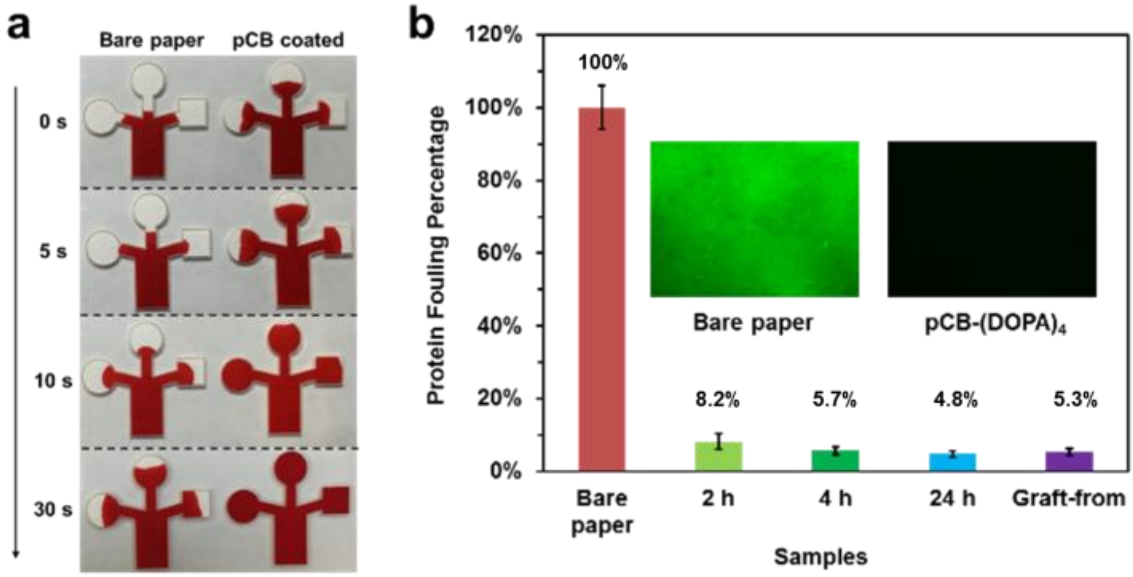

Figure 4.2. a. Comparison of the adsorption of Waterman Red ink by capillary action as a function of time for bare and PCB-$(DOPA)_4$ modified cellulose papers (immersion time: 4 h). b. Amount of adsorbed human fibrinogen (Fb) measured from ELISA on bare, PCB-$(DOPA)_4$ modified (immersion time: 2, 4 or 24 h) and PCB modified (graft-from ATRP method) cellulose papers. Inset: Representative

fluorescence microscopy images of FITC-BSA adsorption onto bare cellulous paper and PCB-$(DOPA)_4$ modified cellulous paper (immersion time: 4 h).

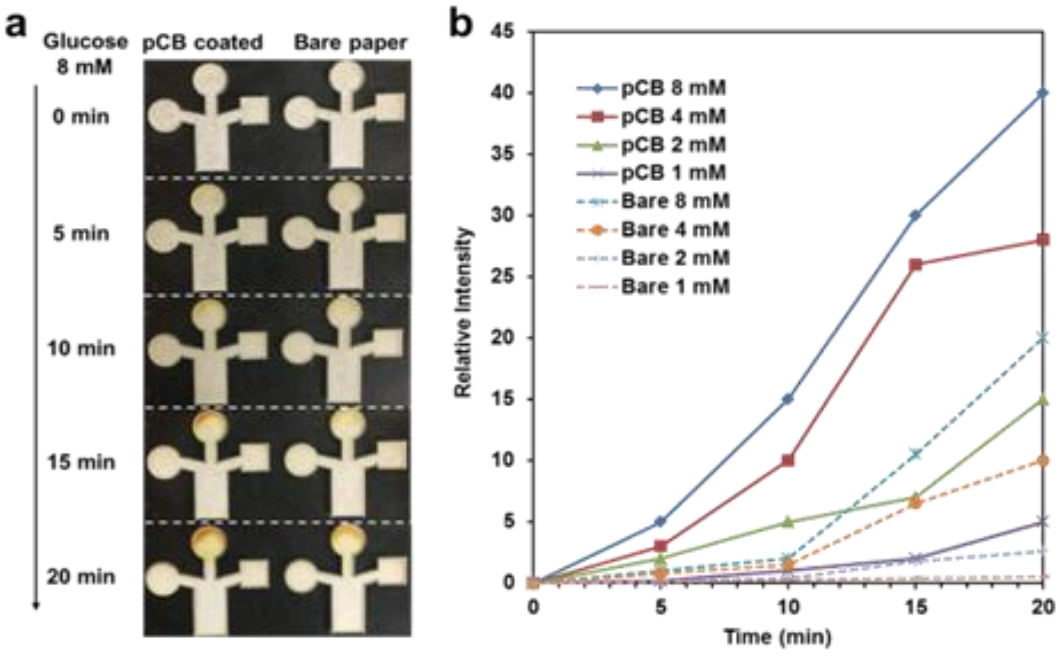

Figure 4.3. a. Glucose detection as a function of time using PCB-$(DOPA)_4$ coated and bare cellulose paper-based analytical devices. Glucose was spiked (8.0 mM) into undiluted human serum. b. The mean relative intensity of the glucose detection zone as a function of time and concentration (1.0 to 8.0 mM) for analysis from undiluted human serum.

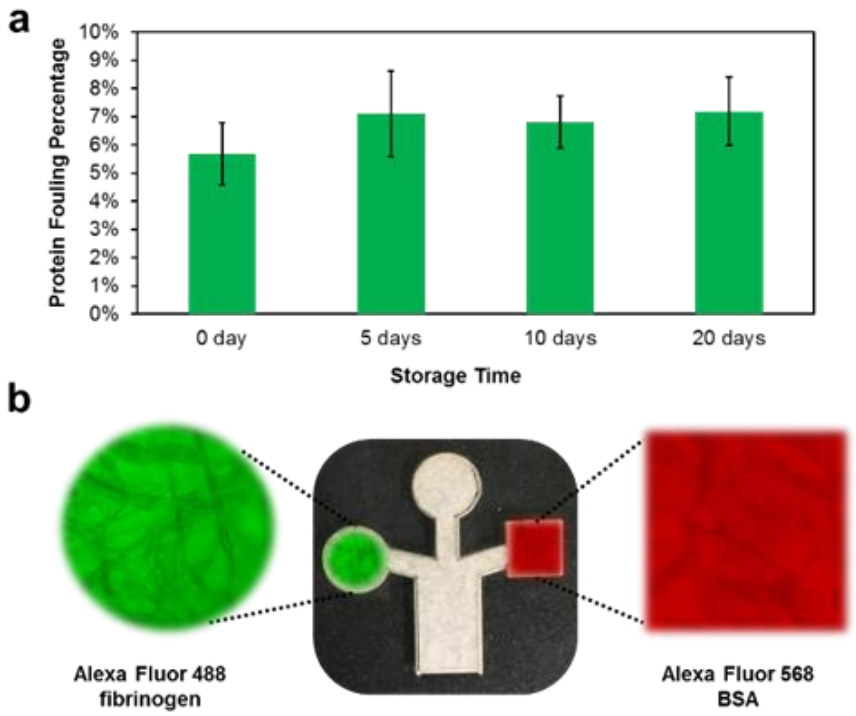

Figure 4.4. a. Normalized amount of adsorbed human fibrinogen (Fb) respective to that on uncoated paper sensor measured from ELISA on PCB-$(DOPA)_4$ modified cellulose paper after storage for 0, 5, 10 and 20 days under room temperature. b. A mixture of fluorescently tagged BSA (red, 50 µg/mL) and fibrinogen (Fb, green, 50 µg/mL) in PBS was wicked through the microfluidic device followed by washing with buffer. The circular region on the left revealed only green fluorescence while the square region on the right revealed only red fluorescence.

Chapter 5 Complement activation on hydrophilic bio-inert polymers

5.1 Introduction

Complement system plays a vital role in the human immune system. It contains over 30 kinds of proteins and plays the role of recognizing and removing of foreign intruders in the human body. The activation of the complement system can be classified into three pathways depending on their activation mechanism. [75-78] The classic pathway (CP) is usually associated with the antigen-antibody interactions, where complement components C1 is activated by recognizing the immune complex. The mannose-binding lectin (MBL) pathway (LP), on the other hand, is normally induced by the specific binding of MBL on to the carbohydrate sugar residue located on the membrane of microorganisms. The alternative pathway (AP) is usually triggered independently of antibody or microorganisms, but by the direct contacting of complement protein onto foreign, especially mam-made, surfaces. Although all these three methods have different initiation steps, they end up with the same key step - the enzymic cleavage of C3 protein in to C3b and C3a and the formation of C3 convertase. All these three activation pathways form the preliminary sensing and transmitting of the dangerous signal of the human innate immune system.

Although the complement system is of great importance in the human immune system, uncontrolled complement can cause a serious health issue such as hypertension, arterial calcification and cardiometabolic risk. [75-78] Complement activation is considered as a vital influence on the biocompatibility of artificial biomaterials." For example the implanted bone materials can trigger the complement. Without the complement regulators on the membrane, foreign materials are easy to trigger the complement reaction when implanted into the human body.

The activation pathway of implanted materials highly depends on the chemical nature of biomaterials. Materials hydrophobicity is one of the critical issues inactivation of complement reaction. Compare to hydrophilic surfaces, hydrophobic surfaces are a more potent activator for complement reaction.. The hydrophobicity of the surfaces results in severe non-specific protein fouling including plasma protein, fibrinogen, and IgG. This bonded protein further triggered the cleaved C3 proteins. Furthermore, the crosstalk between coagulation, fibrinolysis and inflammation system will further amplify this response. Hydrophilic surfaces are well known for their ability in preventing protein fouling, which seems to be able to solve the problems. However, the AP is becoming the dominant mechanism for hydrophilic materials. The current prevailing hydrophilic coating techniques can significantly reduce the fouling of proteins, however, the abundant hydroxyl and amine groups on the material surfaces can form covalent ester or amide bonds with nascent C3b molecules and then trigger the following complement cascade reaction.
Nowadays, a lot of endeavors have been spent the quantification of complement activations on surfaces. However, the current quantification methods of complement reaction lack consistency and are far from flawless. For example, foreign surfaces and gas-liquid interfaces are high complement activator and when doing SPR, the serum is inevitably touching the tubing of the SPR machine and generates a stronger complement reaction than the target surface. On the other hand, there is a lack of direct and standard comparison between commonly used bio-compatible polymers on their complement activation performance.

In this paper, we aim to solve both of these problems at a time. In this study, commonly used polymeric materials were classified into 3 groups based on their functional groups on the polymer backbone, namely, 1. Amino-based materials; 2. Zwitterionic-based materials; and 3.Hydroxyl-based materials. Zwitterionic-based materials, including Carboxybetaine (CB), N-oxide (TMAO) are chosen as the representative to do

the testing. Hydroxyl-based materials are commonly used as non-fouling materials in various medical applications. such as ethylene glycol methacrylate (EGMA), and N-(2-Hydroxypropyl) methacrylamide (HPMA), Also, Amino-based materials, such as monomers bearing primary amine, quaternary amine, tertiary amine are chosen as the candidates to do the test. All these materials were made into polymer hydrogels with 20%wt solid content to make sure the all tested polymer samples have the same amount of functional groups and the hydrogel surfaces is the only surface that the serum contacts with during the incubation. The complement activation level was measured by standard enzyme-linked immunosorbent assay (ELISA)

5.2 Experimental Section

5.2.1 Materials

CB and N-oxide monomer was synthesized according to a previously reported protocol.[15] The following chemicals and materials were purchased from Sigma-Aldrich (St. Louis, MO, USA), and were used as received:, (Hydroxypropyl) methacrylamide (HPMA),Poly(ethylene glycol) methacrylate (PEGMA-OH), Poly(ethylene glycol) methyl ether methacrylate (PEGMA-CH3), 2-(Dimethylamino)ethyl methacrylate (DMAMA), and [2-(Methacryloyloxy)ethyl]trimethylammonium (TMAMA) Ethylene glycol dimethacrylate (EGDMA), 2-Aminoethyl methacrylate hydrochloride (AEMA)

Ethylenediaminetetraacetic acid (EDTA) Phosphate-buffered saline (PBS, 0.01 M phosphate) package, and Whatman 1 filter paper. α-Bromoisobutyryl bromide (BIBB) N,N'-Dicyclohexylcarbodiimide (DCC, 99.8%), ethylene glycol (99.8%), sodium azide (NaN_3, 99%), trifluoromethanesulfonic acid (TfOH, 99%), sodium carbonate (99%), N, N'- diisopropylcarbodiimide (DIPC, 99%), 4-dimethylaminopyridine (DMAP, ≥99%), 4-

Pentynoic acid (98%), 1-thioglycerol (98%), Bovine serum albumin (96%), o-Phenylenediamine (OPD, 98%), N,N-dimethylformamide (anhydrous 99.8%). o-Phenylenediamine (OPD, 98%). The following chemicals and materials were purchased from Thermo Fisher Scientific (Waltham, MA, USA), and were used as received: Dichloromethane (DCM, Reagent grade), hexanes (Certified ACS), tetrahydrofuran (THF,) Toluene (ACS grade), methanol (Reagent grade), N,N-dimethylformamide (anhydrous 99.8%, Sigma-Aldrich), Acetone (Certified ACS). Pooled human blood serum was purchased from BioChemed Services (Winchester, VA, USA). Ethanol (200 proof) was purchased from Decon Labs. Polydimethylsiloxane (PDMS; Sylgard 184) was purchased from Dow Corning. The water used in these experiments was obtained from a Millipore water purification system with a minimum resistivity of 18.0 MΩ cm. Bovine serum albumin (96%), High-impact PS, PVC, PP were purchased from Tapplastics.

5.2.2 Preparation of hydrogel wells

Polymer hydrogels were synthesized by free-radical polymerization. In the first step, the first network poly(carboxybetaine) (PCB) hydrogels were synthesized by photo polymerization using 1 M of carboxybetaine acrylamide(CBAA) monomer, 10 mol% of cross-linker, and 0.1 mol% of 2-hydroxy-2-methylpropiophenone (1173) as initiator (percentages were both relative to the CBAA monomer). 2ml of solution was added into a 24-well plate followed by the insert of a glass tube which 5mm in diameter. The glass tube was mounted concentrically inside the well and 5mm above the bottom of the well, pressing the aqueous solution inside forming a well shape. The aqueous solution was solidified with under an ultraviolet (UV) irradiation with wavelength 305 nm and 6 watt power for 30 min.

The glass tube was then removed from the hydrogel and the hydrogel was immersed in water for 24 hours before use.

5.2.3 Swelling study of hydrogel wells

The prepared hydrogel wells were soaked in the PBS 7.0 solution for 2h, 4h, 8h, respectively, to measure the swelling ratio after soaking. The swelling ratio was calculated by the weight ratio between hydrogel after and before soaking. Hydrogels with different mole fraction(5 mol%, 10 mol%, 20 mol%, 25 mol%, 30 mol%) and crosslink density(5%, 20%,25%, 30%)) was prepared and measured for their swelling ratio.

5.2.4 Complement activation of hydrogel materials via ELISA experiment

Three replicates of hydrogel wells for each material were prepared and soaked in the PBS buffer for 24 hours and was dried with moderate air flow. Then, 300uL of pooled complement human serum (Innovative Research, Novi, MI) was added into replicates of each polymer well and incubated at 37 o C for 90 min and followed by quenching with 30uL of 10mM EDTA solution. Also, during the process, 30ul of serum samples was taken from each wells after 10 min and followed by quenching with 3uL of 10mM EDTA solution for each replicate for C3 complement protein detection. The complement activation degree was measured by quantifying a complement degradation fragment C5b-9 in serum at 90 min and the C3a-desArg after 10min using standard enzyme-linked immunosorbent assay (ELISA) kit (BD Bioscience, San Diego, CA). The complement reaction activated by polymer hydrogels was calculated by deducting the pre-existing C5b-9 in the serum from the obtained C5b-9 concentration from ELISA.

5.3 Results and Discussion

5.3.1 The necessity of hydrogel well preparation

Hydrogels tend to swell when after reaching equilibrium in solutions, resulting in a change of size and mechanical strength. Thus the serum contacting area will be changed. Therefore, the ability for hydrogel well to retain the shape and size after reaching equilibrium in phosphate-buffered saline (similar to physiological condition) was required in this method. After a lot of trial and error test, it is concluded that a hydrogel with 10mol% content and 10% crosslink density is the best combination to achieve both rigidity and unobservable swelling. All wells process a stable and rigid shape with 5mm in diameter and 8mm in depth. **(Figure 5.1)**

Currently, there is still lack a consistent and convincing measurement for complement study and the results are also contradicted to each other. For example, Iwata *et al.* discovered that the amine group is not convincing complement activation group, and there is no direct evidence that the amine group can activate the complement reaction as the hydroxyl groups can do. On the contrary, Lambris et al also concluded that amine group is also a proved complement activator because the amine groups can also attack the thioester bond on the C3b molecule and further activate the complement cascade through the alternative pathway. We propose that the potential reason is that there is still not a consistent measuring method that can effectively eliminate all the environmental factors. For example, C3a-DesArg is the product of C3 cleavage and the measuring of C3a-DesArg can quantitatively reflect the complement activation level of C3 protein. However, the cleavages of C3 protein usually take place at the first 1 to 5 minutes, which makes the measuring impossible to achieve. Also, Iwata *et al.* measured the complement activation

using the self-assemble monolayer (SAM), however, due to the difference of hydrophilicity of SAM, it is hard to achieve an equal contacting area for complement activation. In addition, the flat SAM surface maximized the interfacial area between serum and air, which even weaken the conclusion. Under this circumstance, there is an urgent demand for an effective method that can minimize irrelevant environmental factors. This rigid hydrogel well design enables the control of serum-material interface and the well structure minimizes the serum-air interface. Thus, a consistent and fair measurement can be achieved for current bio-compatible materials.

5.3.4 The complement activation study of different materials.

In this study, CB and N-Oxide were chosen as representatives of zwitterinoic monomers. PEGMA-OH, HPMA, and HEMA are commonly used biomaterials and all of them bears a hydroxyl group on the monomer, which make them potential complement activating materials. PVA was chosen as the positive control as its complement activation ability was already reported. Another version of PEGMA was also chosen in this experiment. PEGMA-CH_3 has a similar molecular weight and similar hydration ability as PEGMA-OH, but the hydroxyl groups was capped with a methyl groups, thus PEGMA-CH_3 was chosen and a comparison to PEGMA-OH to test the complement activation on hydroxyl groups.

All the polymers were made into hydrogel wells with a water content of 80 wt % and a 10% crosslink density. Then, 300 µL of pooled complement human serum was added into each well of polymer hydrogel and incubated at 37 ^{o}C for 10 and 90min. The complement activation degree was then quenched by 50mM EDTA solution.

C5b-9 protein is generated at the very down stream of complement cascade, the activation level of C5b-9 can directly reflect the activation degree of complement reaction. Both zwitterionic polymers showed very low C5b-9 (1.96 μg/mL for PCB and 2..28μg/mL for p(N-oxide)) activations. While all Hydroxyl bearing polymers showed high C5b-9 concentration. It is worth to mention that PEGMA-OH polymer triggered high complement activation (12.16 μg/mL). However, when the OH terminal groups were capped with a CH_3 group, the complement activation was significantly alleviated (5.95 μg/mL). (**Figure 5.3)**This is still higher than the zwitterionic polymers due to its less nonfouling nature. For amino polymers, both tertiary amine (DMAMA) and primary amine (AEMA) shows low complement activation while quaternary amine (TMAMA).The C3a-DesArg level was measured at 10 min after incubation has a consistent result as the C5b-9 concentration, which is another strong evidence of the accuracy of this measurement. **(Figure 5.2)**

5.4 Conclusions

To conclude, we designed a new hydrogel-based method for complement activation measurement. In this method, all the hydrophilic monomers were made into a rigid hydrogel wells with fixed shape, The high solid content and high crosslinking density give the hydrogel wells the identical shape and volume as well as the swell-free feature during the measurement, which enable the consistent measurement and comparison between different materials. Three groups of commonly used biocompatible polymers with different functional groups, namely, amino-based, zwitterionic-based, and hydroxyl-based polymers were tested using this method. Zwitterionic materials show the lowest complement activation level and lowest protein fouling among other materials. Hydroxyl-bearing materials, although have good antifouling properties, however, the high complement

activating ability impedes their further application in the field of biomaterials and biopharmaceuticals.

5.5 Figures

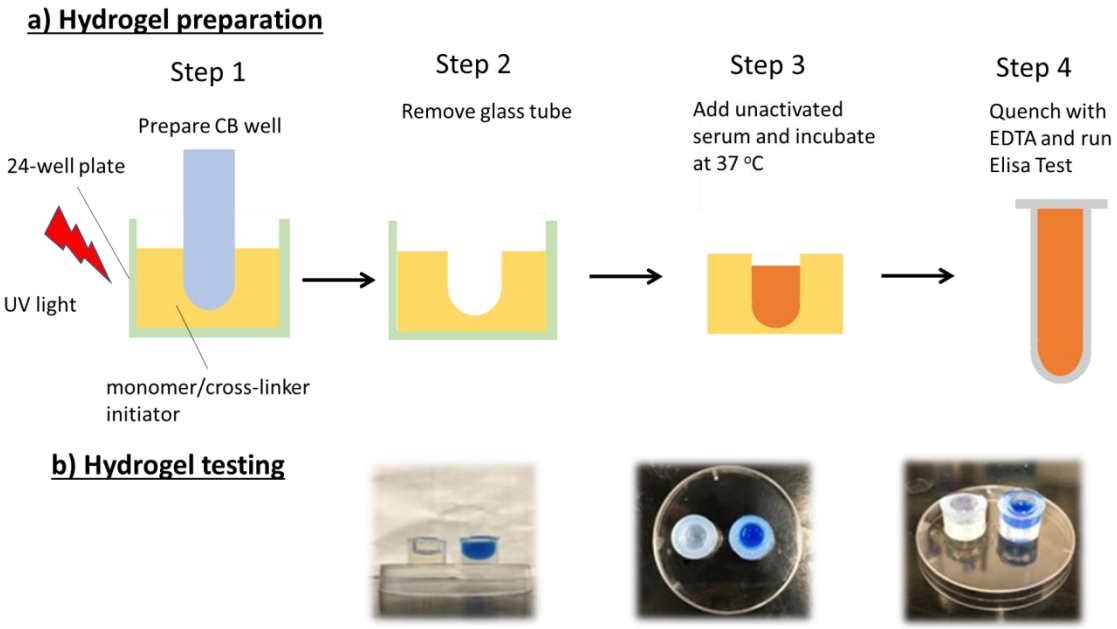

Figure.5.1. a) Hydrogel well preparation, b) Hydrogel well filled with blue ink.

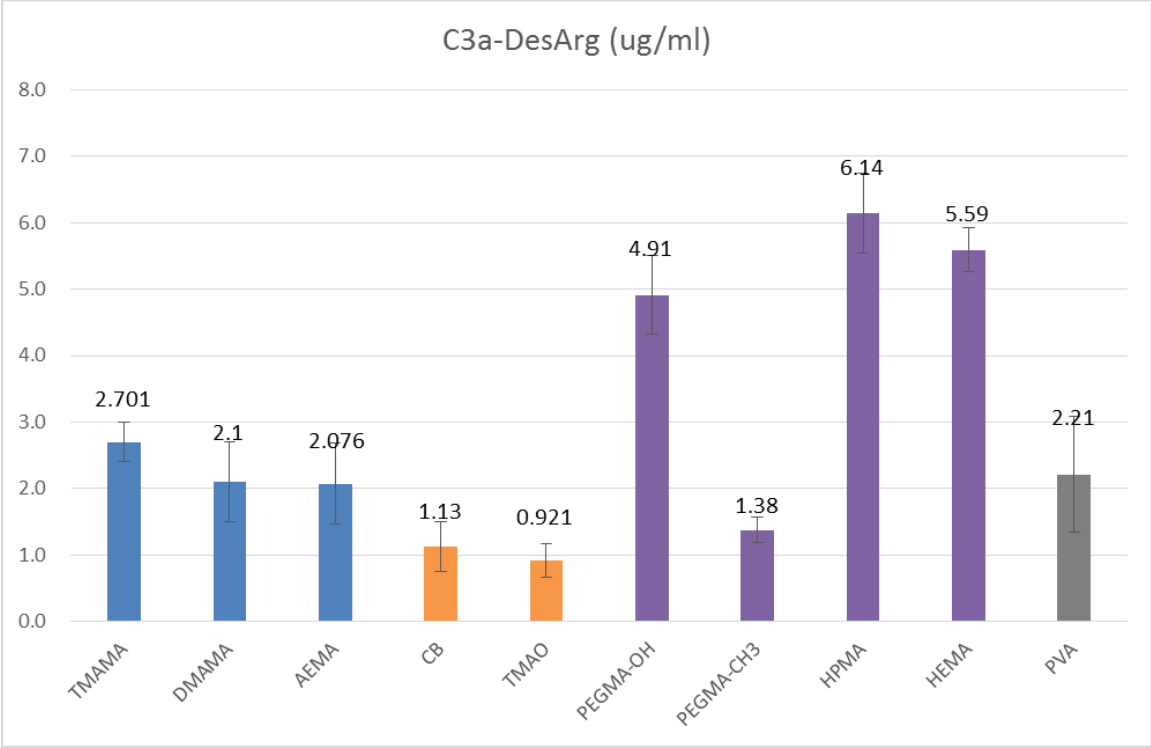

Figure 5.2. C3a-DesArg concentration after 10 min incubation.

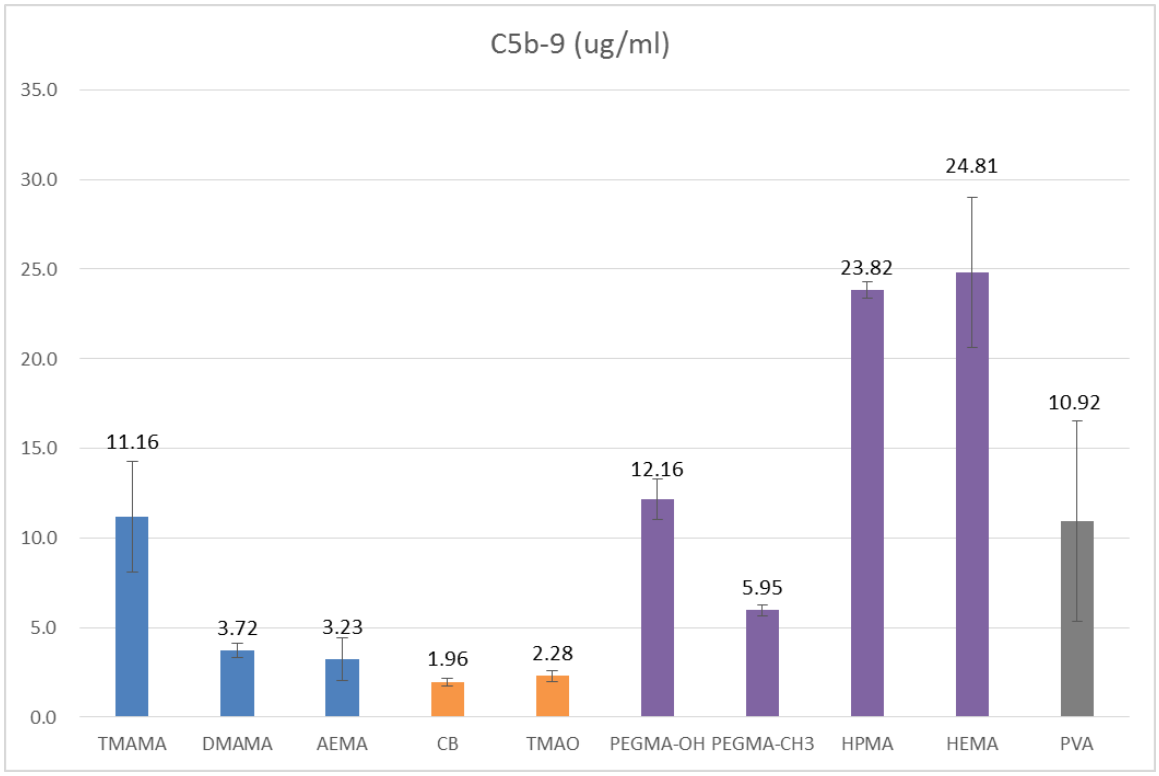

Figure 5.3. C5b-9 concentration after 90 min incubation.

Chapter 6 Current Conclusions and Future Work

6.1 Current Conclusions

Chapter 6 Current Conclusions and Future Work

6.1 Current Conclusions

This thesis explores and investigates the strategies to improve the performance of zwitterionic non-fouling coatings through a “graft-to” method. The molecular design principles of coating molecules are described. The newly developed “graft-to” technology is applied to artificial blood contacting devices. In addition, a new and accurate surface-induced complement activation method using polymer hydrogel is demonstrated which can be used to quantitatively measure the complement activation and eliminate the intervention from environmental factors.

The first part of the thesis (Chapter 2-3) focused on how we develop a new universal “graft-to” technology and applied this new technology to blood-contacting respiratory devices. In chapter 2, we prepared a series of zwitterionic PCB-DOPA conjugates of (PCB)m-(DOPA)n with the different number of PCB chains (m) and DOPA binding groups (n). By manipulating the combination of m and n, we systematically investigated the structural effect on the coating performance. All the measurements, such as ELISA, bacteria attachment test as well as SPR confirmed that the increasing of DOPA binding groups number leads to a more denser and more effective coating, while the star-shaped polymer structure can further increase the performance of the coating. This resulting “Janus” form star-shaped molecule (n=4, m=4) showed the lowest protein adsorption of 19.5 ng/cm2 against 100% human serum from measurements with a surface plasmon resonance (SPR)

sensor, which is the lowest result achieved by any surface–independent "graft-to" zwitterionic coating to the best of our knowledge. In chapter 3, PCB-$(DOPA)_4$ conjugate was applied to the artificial lung devices and significantly reduced the blood flow resistance and the device failure over 36-hours compared to the uncoated samples. In the 4-hour rabbit study, PCB-$(DOPA)_4$ coating also showed a higher activated clotting time of 220-300s (N $\geqslant$5), reduced fibrin formation ($p=0.06$) and gross thrombus formation by 59% ($p<0.05$) compares to the uncoated control.

The second part of the thesis (Chapter 4) emphasized how the combination of "dip-coating" and protein immobilization can increase the performance and reduce the cost of the biosensors. In this part, we applied a zwitterionic PCB polymer conjugated with four DOPA adhesive groups via dip-coating to cellulose paper sensors, rendering nonfouling properties and improving detection in complex media. Results demonstrate that this dip-coating process is much simpler and more convenient than the previously reported "graft-from" SI-ATRP method and achieves similar hydrophilicity and nonfouling performance. The coated paper sensor showed accelerated diffusion of analyte and improved sensitivity of glucose detection, particularly in real-world complex media such as human blood serum. We further demonstrated the capability of PCB-$(DOPA)_4$ modified paper sensors for the specific detection of antigens after covalently immobilizing antibodies on PCB surfaces. In addition, these coatings are showed to be stable for more than 20 days.

The third part of the thesis (Chapter 5) focused on the immunogenicity of current bio-materials. In this part, we designed a new hydrogel-based method for complement activation measurement. This method, all the hydrophilic monomers were made into 20%wt hydrogel wells, all the wells processed the same crosslink density of 10% with

EGDMA as the crosslinker. This high solid content and high crosslinking density give the hydrogel wells the same shape and same volume as well as the non-deformable feature during the measurement, which enable the consistent measurement and comparison between different materials. Three groups of commonly used biocompatible polymers with different functional groups, namely, amino-based, zwitterionic-based, and hydroxyl-based polymers were tested using this method and zwitterionic materials show the lowest complement activation level and lowest protein fouling among other materials. Hydroxyl-bearing materials, although have good antifouling properties, however, the high complement activating ability impedes their further application in the field of biomaterials and biopharmaceuticals.

6.2 Future Work

6.2.1 Evaluation of organ cellular toxicity of PCB-DOPA conjugates

We have successfully developed the PCB-DOPA conjugates as a non-fouling coating material and applied it into a real application. In vivo sheep study demonstrated that this PCB-DOPA conjugates effectively reduced the thrombus formation and inhibits the blood coagulation compare with untreated devices. As a non-biodegradable blood-contacting material, we are also interested to evaluate its stability under blood shear force and associated toxicity. The next step of this project is to evaluate the cytotoxicity of this coating using the ISO Elution Method. Experimentally, PCB-DOPA with 100 kDa molecular weight will be coated onto each well of a 12-well TCPS plate. The blank well of a TCPS plate incubated in normal media can be used as negative control while a small piece of latex (cut from a pipette bulb and sterilized in 70% ethanol) can be used as a

positive control for cytotoxicity. The L929 or NIH3T3 cells will be incubated in the coated and control wells at 37C for 12/24/48 hours and then subjected to microscope examination. The cytotoxicity will be rated on a reactivity grade from 0 to 4 using guidelines developed by the US Pharmacopcia (USP) or ISO 10993-5 by observing cells for any visible change from normal morphology compared to the negative control cells.

6.2.2 Simplification of PCB-DOPA conjugates synthesis

This thesis is mainly focused on the development of new material to improve coating performance and increase the biocompatibility of artificial devices. As discussed above, this PCB-DOPA conjugates has been proven to be effective on artificial lung devices. However, the synthesis route is still complicated and time-consuming, which imped its real application. The structure discussion proved that the multi-binding groups and the crosslinking strategy are the key factors to achieve a universal binding and high coating density. A simplified version of PCB-DOPA conjugates was proposed as shown in scheme 6.1. A PCB-(DOPA)3 with a simplified version linker structure will be prepared and synthesized.

6.2.3 The effect of nanomedicine corona on complement activation and nanoparticle circulation time

Biopharmaceutical drugs, including peptides, proteins, monoclonal antibodies, drug-antibody conjugates and aptamers, offer significant advantages over small molecule therapeutics due to their specific bioactivity and high potency. Despite the huge success achieved by biopharmaceutics, these structurally complex biomacromolecules usually face

great challenges including instability, short circulation half-life and immunogenicity. A short half-life limits therapeutic efficacy while unfavorable immune responses not only result in accelerated blood clearance during chronic use, but also cause anaphylaxis and infusion reactions.

As we know, complement reaction plays an important role in human innate and adaptive immune system. The clearance of biopharmaceutical drugs can be classified into three categories: (i) disintegration of nanoparticles by protein adsorption, (ii) opsonization - mediated nanoparticle removal by immune cells, and (iii) filtration by organs with fenestrated vasculature. The activation of complement protein plays an important role in the rapid clearance of bio-pharmaceutics and leads to a short circulation time. Also, antibodies can also activate the complement via the classical pathway, resulting in deposition of C3b and C4b onto the antigen surface. After C3b has bound to the surface of an antigen, it can be recognized by phagocyte receptors that signal for phagocytosis. Ishida *et al.* demonstrates the complement system is a key factor in the accelerated blood clearance of nano-particles.[75]

Conjugating polyethylene glycol (PEG) to proteins, known as PEGylation, is thus far the most successful tactic used to modify therapeutic proteins. The chemically conjugated PEG molecules increase the overall hydrodynamic size of the bioconjugates to avoid renal excretion and extend vascular residence time. The hydrated flexible PEG chains also reduce immune recognition by sterically shielding protein epitopes and resist non-specific protein adsorptions. However, this technique is still not flawless in terms of complement activation. Hubbell *et al.* discovered the exposure of hydroxyl OH groups can trigger heavy

complement activation. Thus, there is a real demand to investigate the influence of complement activation in biopharmaceutical application. [76-80]

The complement activation property of different materials has been characterized in chapter 4 and it is time to find out how these properties can actual help to improve the design of biopharmaceutics. In this proposed work, we hypothesize that even the PEGylation can increase circulation time of modify therapeutic proteins to some degree, the pendant OH groups on the corona of protein-conjugate can still potentially activate the complement reaction and accelerate the clearance of therapeutic proteins. While PCB can protect the protein from both protein adsorption and complement related opsonization.

We intend to study the innate immune response instead of the adaptive immune response of PCB by monitoring the circulation time after the first injection of PCB-conjugates, PEGMA-conjugates, and PEG-conjugate. Complement activation degree will be determined by the measuring of protein C3a and C5b-9 at 10 min and 90 min after the injection. Organs distribution, such as spleen, liver, and kidney will be examined for cytoplasmic vacuoles through histology staining for different corona polymers. In this work, we wish to further evaluate the complement activation of different polymers for biological drug delivery.

6.3 **Figures**

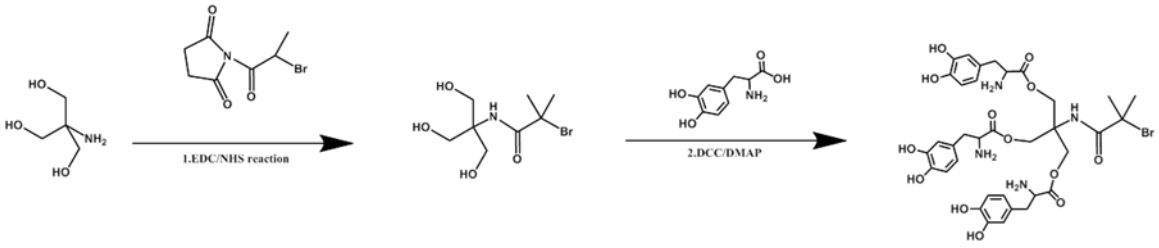

Scheme 6.1: Simplified PCB-DOPA conjugate route.

Reference

[1] a) W. Qiang, B. Tobias, A. U. Stefano, D. Joachim, W. Christian, N. A. T., L. Andreas, B. Matthias, H. Rainer, *Angewandte Chemie International Edition* **2014**, 53, 8004; b) S. Krishnan, C. J. Weinman, C. K. Ober, *Journal of Materials Chemistry* **2008**, 18, 3405; c) S.-H. Ye, D. T. Arazawa, Y. Zhu, V. Shankarraman, A. D. Malkin, J. D. Kimmel, L. J. Gamble, K. Ishihara, W. J. Federspiel, W. R. Wagner, *Langmuir* **2015**, 31, 2463.

[2] a) S. G. Boyes, A. M. Granville, M. Baum, B. Akgun, B. K. Mirous, W. J. Brittain, *Surface Science* **2004**, 570, 1; b) D. Hong, H.-C. Hung, K. Wu, X. Lin, F. Sun, P. Zhang, S. Liu, K. E. Cook, S. Jiang, *ACS Applied Materials & Interfaces* **2017**, 9, 9255; c) X. Lin, T. Konno, M. Takai, K. Ishihara, *Colloids and Surfaces B: Biointerfaces* **2013**, 102, 857; d) X. Lin, K. Fukazawa, K. Ishihara, *ACS Applied Materials & Interfaces* **2015**, 7, 17489.

[3] a) S. Seo, S. Das, P. J. Zalicki, R. Mirshafian, C. D. Eisenbach, J. N. Israelachvili, J. H. Waite, B. K. Ahn, *Journal of the American Chemical Society* **2015**, 137, 9214; b) Q. Lu, E. Danner, J. H. Waite, J. N. Israelachvili, H. Zeng, D. S. Hwang, *Journal of The Royal Society Interface* **2013**, 10.

[4] a) L. Pan, H. Wang, C. Wu, C. Liao, L. Li, *ACS Applied Materials & Interfaces*

2015, 7, 16003; b) S. M. Kang, J. Rho, I. S. Choi, P. B. Messersmith, H. Lee, *Journal of the American Chemical Society* **2009**, 131, 13224.

[5] H. Lee, S. M. Dellatore, W. M. Miller, P. B. Messersmith, *Science* **2007**, 318, 426.

[6] S. Qing, J. Shaoyi, *Advanced Materials* **2015**, 27, 15.

[7] H. S. Sundaram, X. Han, A. K. Nowinski, J.-R. Ella-Menye, C. Wimbish, P. Marek, K. Senecal, S. Jiang, *ACS Applied Materials & Interfaces* **2014**, 6, 6664.

[8] H. S. Sundaram, X. Han, A. K. Nowinski, N. D. Brault, Y. Li, J.-R. Ella-Menye, K. A. Amoaka, K. E. Cook, P. Marek, K. Senecal, Jiang, S. *Advanced Materials Interfaces* **2014**, 1, 1400071.

[9] a) J. D. Badjić, A. Nelson, S. J. Cantrill, W. B. Turnbull, J. F. Stoddart, *Accounts of Chemical Research* **2005**, 38, 723; b) F. Carlo, S. C. A., W. Marcus, S. Oliver, H. Stefan, K. Beate, D. Jens, G. Christina, K. Ernst‐Walter, H. Rainer, *Angewandte Chemie International Edition* **2012**, 51, 10472.

[10] G. Lapienis, *Progress in Polymer Science* **2009**, 34, 852.

[11] a) K. Yue, C. Liu, K. Guo, K. Wu, X.-H. Dong, H. Liu, M. Huang, C. Wesdemiotis, S. Z. D. Cheng, W.-B. Zhang, *Polymer Chemistry* **2013**, 4, 1056; b) Z. Lin, P. Lu, X. Yu, W.-B. Zhang, M. Huang, K. Wu, K. Guo, C. Wesdemiotis, X. Zhu, Z. Zhang, K. Yue, S. Z. D. Cheng, *Macromolecules* **2014**, 47, 4160; c) E. R. Gillies, J. M. J. Fréchet, *Journal of the American Chemical Society* **2002**, 124, 14137; d) K. Wu, M. Huang, K. Yue, C. Liu, Z. Lin, H. Liu, W. Zhang, C.-H. Hsu, A.-C. Shi, W.-B. Zhang, S. Z. D. Cheng, *Macromolecules* **2014**, 47, 4622.

[12] R. K. Iha, K. L. Wooley, A. M. Nyström, D. J. Burke, M. J. Kade, C. J. Hawker, *Chemical Reviews* **2009**, 109, 5620.

[13] A. J. Keefe, N. D. Brault, S. Jiang, *Biomacromolecules* **2012**, 13, 1683.

[14] S. Chen, S. Jiang, *Advanced Materials* **2008**, 20, 335.

[15] C. Zhiqiang, Y. Qiuming, X. Hong, C. Gang, J. Shaoyi, *Angewandte Chemie International Edition* **2010**, 49, 3771.

[16] Murphy, S. L., Xu, J., Kochanek, K. D., Curtin, S. C. & Arias, E. Deaths: Final data for 2015. *Natl. Vital Stat. Reports* **66,** (2017).

[17]. *Cystic Fibrosis Foundation Patient Registry 2016 Annual Data Report*. (2017).

[18] Olson, A. L. *et al.* Mortality from Pulmonary Fibrosis Increased in the United States

from 1992 to 2003. *Am. J. Respir. Crit. Care Med.* **176,** 277–284 (2007).

[19]. Hutchinson, J. P., McKeever, T. M., Fogarty, A. W., Navaratnam, V. & Hubbard, R. B. Increasing global mortality from idiopathic pulmonary fibrosis in the twenty-first century. *Ann. Am. Thorac. Soc.* **11,** 1176–1185 (2014).

[20]. Valapour, M. *et al.* OPTN/SRTR 2016 Annual Data Report: Lung. *Am. J. Transplant.* **18,** 363–433 (2018).

[21]. Fischer, S. *et al.* Bridge to lung transplantation with the novel pumpless interventional lung assist device NovaLung. *J. Thorac. Cardiovasc. Surg.* **131,** 719–723 (2006).

[22]. Haneya, A. *et al.* Extracorporeal Circulatory Systems as a Bridge to Lung Transplantation at Remote Transplant Centers. *Ann. Thorac. Surg.* **91,** 250–255 (2011).

[23]. Maul, T. M. ECMO Anticoagulation : It's Still the Biggest Challenge ! in *ASAIO 61st Annual Conference* (2015).

[24]. Dalton, H. J. *et al.* Association of bleeding and thrombosis with outcome in Extracorporeal Life Support. *Pediatr. Crit. Care Med.* **16,** 167–174 (2015).

[25] Mazzeffi, M. *et al.* Bleeding, Transfusion, and Mortality on Extracorporeal Life Support: ECLS Working Group on Thrombosis and Hemostasis. *Ann. Thorac. Surg.* **101,** 682–689 (2016).

[26]. Gorman, R. C. *et al.* Surface-bound heparin fails to reduce thrombin formation during clinical cardiopulmonary bypass. *J. Thorac. Cardiovasc. Surg.* **111,** 1–12 (1996).

[27]. Park, K., Shim, H. S., Dewanjee, M. K. & Eigler, N. L. In vitro and in vivo studies of PEO-grafted blood-contacting cardiovascular prostheses. *J. Biomater. Sci. Polym. Ed.* **11,** 1121–1134 (2000).

[28]. Kidane, A., Lantz, G. C., Jo, S. & Park, K. Surface modification with PEO-containing triblock copolymer for improved biocompatibility: In vitro and ex vivo studies. *J. Biomater. Sci. Polym. Ed.* **10,** 1089–1105 (1999).

[29]. Ladd, J., Zhang, Z., Chen, S., Hower, J. C. & Jiang, S. Zwitterionic polymers exhibiting high resistance to nonspecific protein adsorption from human serum and plasma. *Biomacromolecules* **9,** 1357–1361 (2008).

[30]. Hong, D. *et al.* Achieving Ultralow Fouling under Ambient Conditions via Surface-Initiated ARGET ATRP of Carboxybetaine. *ACS Appl. Mater. Interfaces* **9,** 9255–9259 (2017).

[31]. Sundaram, H. S. *et al.* Achieving One-Step Surface Coating of Highly Hydrophilic Poly(Carboxybetaine Methacrylate) Polymers on Hydrophobic and Hydrophilic Surfaces. *Adv. Mater. Interfaces* **1,** n/a-n/a (2014).

[32]. Amoako, K. A., Sundaram, H. S., Suhaib, A., Jiang, S. & Cook, K. E. Multimodal, Biomaterial-Focused Anticoagulation via Superlow Fouling Zwitterionic Functional Groups Coupled with Anti-Platelet Nitric Oxide Release. *Adv. Mater. Interfaces* **3,** 1–9 (2016).

[33]. Jiang, S. Y. & Cao, Z. Q. Ultralow-fouling, functionalizable, and hydrolyzable zwitterionic materials and their derivatives for biological applications. *Adv. Mater.* **22,** 920–932 (2010).

[34]. Sun, F. *et al.* Paper Sensor Coated with a Poly(carboxybetaine)-Multiple DOPA Conjugate via Dip-Coating for Biosensing in Complex Media. *Anal. Chem.* **89,** 10999–11004 (2017).

[35]. Zhang, Z. *et al.* Nonfouling Behavior of Polycarboxybetaine-Grafted Surfaces: Structural and Environmental Effects. *Biomacromolecules* **9,** 2686–2692 (2008).

[36]. Lin, X., Konno, T. & Ishihara, K. Cell-Membrane-Permeable and Cytocompatible Phospholipid Polymer Nanoprobes Conjugated with Molecular Beacons. *Biomacromolecules* **15,** 150–157 (2014).

[37]. Lin, X., Fukazawa, K. & Ishihara, K. Photoreactive Polymers Bearing a Zwitterionic Phosphorylcholine Group for Surface Modification of Biomaterials. *ACS Appl. Mater. Interfaces* **7,** 17489–17498 (2015).

[38]. Lin, X., Fukazawa, K. & Ishihara, K. Photoinduced inhibition of DNA unwinding in vitro with water-soluble polymers containing both phosphorylcholine and photoreactive groups. *Acta Biomater.* **40,** 226–234 (2016).

[39]. Kord Forooshani, P. & Lee, B. P. Recent approaches in designing bioadhesive materials inspired by mussel adhesive protein. *J. Polym. Sci. A. Polym. Chem.* **55,** 9–33 (2017).

[40]. Lee, H., Scherer, N. F. & Messersmith, P. B. Single-molecule mechanics of mussel

adhesion. *Proc. Natl. Acad. Sci.* **103,** 12999 LP-13003 (2006).

[41]. Ishihara, K. Bioinspired phospholipid polymer biomaterials for making high performance artificial organs. *Sci. Technol. Adv. Mater.* **1,** 131–138 (2000).

[42]. Chen, S. H., Chang, Y. & Ishihara, K. Reduced blood cell adhesion on polypropylene substrates through a simple surface zwitterionization. *Langmuir* **33,** 611–621 (2017).

[43]. Lai, A. *et al.* Short Term in vivo Evaluation of Nitric Oxide Generating Artificial Lung in Sheep. in *ASAIO 63rd Annual Conference Abstracts* 112 (2017).

[44]. Ye, S.-H. *et al.* Hollow Fiber Membrane Modification with Functional Zwitterionic Macromolecules for Improved Thromboresistance in Artificial Lungs. *Langmuir* 150223065126005 (2015). doi:10.1021/la504907m

[45]. Thorsen, S. The Mechanism of Plasminogen Activation and the Variability of the Fibrin Effector during Tissue‐type Plasminogen Activator—mediated Fibrinolysis. *Ann. N. Y. Acad. Sci.* **667,** 52–63 (1992).

[46]. Borgdorff, P., Fekkes, D. & Tangelder, G. J. Hypotension Caused by Extracorporeal Circulation. *Circulation* **106,** 2588 LP-2593 (2002).

[47]. Linneweber, J., Chow, T. W., Kawamura, M., Moake, J. L. & Nosè, Y. In Vitro Comparison of Blood Pump Induced Platelet Microaggregates between a Centrifugal and Roller Pump During Cardiopulmonary Bypass. *Int. J. Artif. Organs* **25,** 549–555 (2002).

[48]. Shen, M. *et al.* PEO-like plasma polymerized tetraglyme surface interactions with leukocytes and proteins: In vitro and in vivo studies. *J. Biomater. Sci. Polym. Ed.* **13,** 367–390 (2002).

[49]. Yang, W. *et al.* The effect of lightly crosslinked poly(carboxybetaine) hydrogel coating on the performance of sensors in whole blood. *Biomaterials* **33,** 7945–7951 (2012).

[50]. Martinez, A. W.; Phillips, S. T.; Butte, M. J.; Whitesides, G. M. *ANGEW CHEM INT EDIT* **2007**, *46*, 1318-1320.

[51]. Martinez, A. W.; Phillips, S. T.; Whitesides, G. M.; Carrilho, E. *Anal Chem* 2010, 82, 3-10.

[52]. Cheng, C. M.; Martinez, A. W.; Gong, J.; Mace, C. R.; Phillips, S. T.; Carrilho, E.; Mirica, K. A.; Whitesides, G. M. *ANGEW CHEM INT EDIT* 2010, 49, 4771-4774.

[53]. Fu, E.; Liang, T.; Houghtaling, J.; Ramachandran, S.; Ramsey, S. A.; Lutz, B.; Yager, P. *Anal Chem* 2011, 83, 7941-7946.

[54]. Li, X.; Ballerini, D. R.; Shen, W. Biomicrofluidics 2012, 6, 011301.

[55]. Joos, T. O.; Schrenk, M.; Höpfl, P.; Kröger, K.; Chowdhury, U.; Stoll, D.; Schörner, D.; Dürr, M.; Herick, K.; Rupp, S. *Electrophoresis* 2000, 21, 2641-2650.

[56] Liotta, L. A.; Espina, V.; Mehta, A. I.; Calvert, V.; Rosenblatt, K.; Geho, D.; Munson, P. J.; Young, L.; Wulfkuhle, J.; Petricoin, E. F. *Cancer Cell* 2003, 3, 317-325.

[57]. Zhu, Y.; Xu, X.; Brault, N. D.; Keefe, A. J.; Han, X.; Deng, Y.; Xu, J.; Yu, Q.; Jiang, S. *Anal Chem* 2014, 86, 2871-2875.

[58]. Yang, W.; Xue, H.; Li, W.; Zhang, J.; Jiang, S. *Langmuir* 2009, 25, 11911-11916.

[59]. Zhang, Z.; Chen, S.; Jiang, S . *Biomacromolecules* 2006, 7, 3311-3315.

[60]. Vaisocherova, H.; Yang, W.; Zhang, Z.; Cao, Z.; Cheng, G.; Piliarik, M.; Homola, J.; Jiang, S.; *Anal Chem* **2008**, 80, 7894-7901.

[61]. Brault, N. D.; Sundaram, H. S.; Li, Y.; Huang, C.-J.; Yu, Q.; Jiang, S. *Biomacromolecules* **2012,** 13, 589-593.

[62]. Keefe, A.; Brault, N.D.; Jiang, S. *Biomacromolecules,* 2012, 13, 1683-1687.

[63]. Huang, C.-F. *Polymer Journal* **2016**, 341–350

[64]. Kong, B.; Choi, J. S.; Jeon, S.; Choi, I. S. *Biomaterials* **2009**, 30, 5514-5522.

[65]. Gao, C.; Li, G.; Xue, H.; Yang, W.; Zhang, F.; Jiang, S. *Biomaterials* 2010, 31, 1486-1492.

[66]. Sundaram, H. S.; Han, X.; Nowinski, A. K.; Ella-Menye, J.-R.; Wimbish, C.; Marek, P.; Senecal, K.; Jiang, S. *Acs Appl Mater Inter* **2014**, 6, 6664-6671.

[67]. Zhu, Y.; Sundaram, H. S.; Liu, S.; Zhang, L.; Xu, X.; Yu, Q.; Xu, J.; Jiang, S. *Biomacromolecules* 2014, 15, 1845-1851.

[68]. Wei, W.; Yu, J.; Broomell, C.; Israelachvili, J. N.; Waite, J. H. *J Am Chem Soc* 2012, 135, 377-383.

[69]. Lee, H.; Dellatore, S. M.; Miller, W. M.; Messersmith, P. B. *Science* 2007, 318, 426-430.

[70]. Sileika, T. S.; Barrett, D. G.; Zhang, R.; Lau, K. H. A.; Messersmith, P. B. *ANGEW CHEM INT EDIT* 2013, 52, 10766-10770.

[71]. Kim, S.; Gim, T.; Kang, S. M. *Acs Appl Mater Inter,* 2015, 7, 6412-6416.

[72]. Zhang, Z.; Vaisocherova, H.; Cheng, G.; Yang, W.; Xue, H.; Jiang, S. *Biomacromolecules* 2008, 9, 2686-2692.

[73]. Sundaram, H.S.; Han, X.; Nowinski, A.K.; Brault, N.D.; Li, Y.; Ella-Menye J-R.; Amoaka, K.A.; Cook, K.E.; Marek, P.; Senecal, K.; Jiang, S. *Acs Appl Mater Inter*, 2014, 1, 140071.

[74]. Tang, W.; Policastro, G. M.; Hua, G.; Guo, K.; Zhou, J.; Wesdemiotis, C.; Doll, G. L.; Becker, M. L. *J Am Chem Soc* 2014, 136, 16357-16367.

[75]. Taro S, Amr S. Abu L', Risako F'a, Mizuki A, Munehira K, Yosuke H, Keiichiro Oa, Yu I, T, Ishida, *European Journal of Pharmaceutics and Biopharmaceutics,* 127, 2018, 142-149,

[76]. S， T Reddy, A， J Vlies, E, Simeoni, V, Angeli, G, J Randolph, C, P O'Neil, L, K Lee, M, A S,y A Hubbell *Nature Biotechnology* **2007**, 25, 1159-1164

[77]. F, Poppelaars; B, Faria; M, Costa; C, F. M. F, W, J. van Son; S, P. Berger; M, R. Daha; M, A. Seelen.. *Front Immunol*. **2018**,9,71.

[78]. Y, Arima; M, Kawagoe; M, Toda; H, Iwata. Complement Activation by Polymers Carrying Hydroxyl Groups. *ACS Applied Materials & Interfaces* **2009,** 1 (10), 2400-2407.

[79]. FChen; G Wang; JI. Griffin; B Brenneman; N K. Banda; V. M. Holers; D. S. Backos; L. Wu; S. M. Moghimi; D. Simberg. *Nature Nanotechnology*. **2017**, 12, 387–393.

Curriculum Vitae

Kan Wu

EDUCATION

2014 – 2020	University of Washington, Seattle, WA Ph.D. in Chemical Engineering, June 2020
2012 – 2014	University of Akron, Akron, OH M.S. in polymer science
2009 – 2012	Donghua University, Shanghai, China B.S. in Materials Science and Engineering

PUBLICATIONS

***Equal contribution*

1. **K, W**; X, Che; H, Hung; Z, Yuan; P, Zhang; X, Lin, P, Jain, C, Tsao; B, Li; S, Jiang Understanding the structure of pCB-DOPA conjugates towards a universal non-fouling coating *Advanced Functional Materials* In preparation

2. **K, Wu**; X, Lin; H,Xu; Q,, Zhou; P, Zhang; B, Li; C, Tsao; R, Buddy; S, Jiang Complement reactions towards synthetic biocompatible materials *In preparation*

3. **K, Wu*,** F, Sun*, H, Hung, P, Zhang, X, Che, J, Smith, X, Lin, B, Li, P, Jain, Q,Yu, S, Jiang, Paper sensor coated with a poly (carboxybetaine)-multiple DOPA conjugate via dip-

coating for biosensing in complex media *Analytical chemistry* 89 (20), 10999-11004

4. R, Ukita, **K, Wu**, X, Lin, N, M Carleton, N, Naito, A, Lai, C, Do-Nguyen, C, T Demarest, S, Jiang, K, Cook Zwitterionic poly-carboxybetaine coating reduces artificial lung thrombosis in sheep and rabbits *Acta biomaterialia* 92, 71-81

5. X, Lin, P, Jain, **K, Wu**, D, Hong, H, Hung, M, O'Kelly, B, Li, P, Zhang, Z, Yuan, Shaoyi Jiang Ultralow fouling and functionalizable surface chemistry based on zwitterionic carboxybetaine random copolymers *Langmuir* 35 (5), 1544-1551

6. P, Zhang; P Jain; C, Tsao; K, Wu; S Jiang Proactively Reducing Anti‐Drug Antibodies via Immunom,odulatory Bioconjugation *Angewandte Chemie* 131 (8), 2455-2458

7. X, Lin; **Kan Wu**; Q, Zhou; P, Jain; M, O'Kelly; B, Li; H, Hung; S, Creason; J, Himmelfarb; B, D Ratner; S, Jiang Photoreactive Carboxybetaine Copolymers Impart Biocompatibility and Inhibit Plasticizer Leaching on Polyvinyl Chloride *ACS Applied Materials & Interfaces* 12 (37), 41026-41037

8. K, Wu; M, Huang; K, Yue; C, Liu, Z, Lin; H, Liu; W, Zhang; C, Hsu; A, Shi; W, Zhang; Stephen ZD Cheng Asymmetric giant "bolaform-like" surfactants: precise synthesis, phase diagram, and crystallization-induced phase separation *Macromolecules* 47 (14), 4622-4633